AD-A191 979 STRESS CORROSION OF CERAMIC MATERIALS(U) NATIONAL BUREAU OF STANDARDS GAITHERSBURG MD CERAMICS DIV S W FREIMAN ET AL. 10 JAN 88 N00014-87-F-0007 1/1

UNCLASSIFIED F/G 11/2 NL

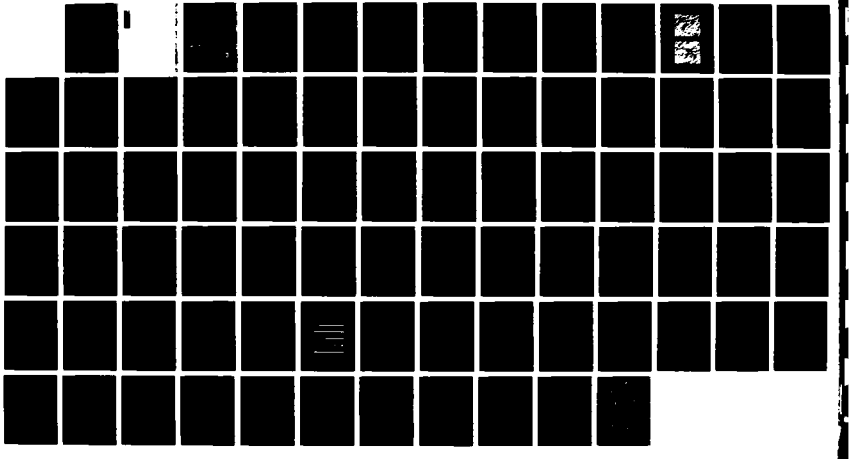

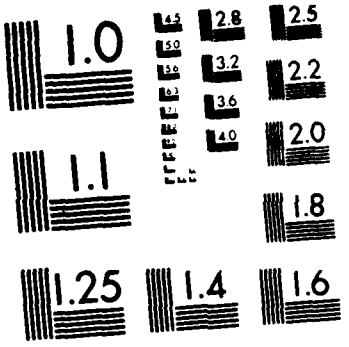

Table of Contents

STRESS CORROSION OF CERAMIC MATERIALS

SUMMARY

The work during fiscal year 1987 can be divided into two distinct areas, namely (1) the fundamental mechanisms involved in environmentally enhanced fracture of single crystals, and (2) fracture behavior of ceramics used in multilayer capacitors. The results of these investigations are summarized as follows:

(1) Environmentally Enhanced Crack Growth

Background:

Previous work concerning silica based glass and sapphire, both about 70% ionic, and MgF_2, essentially 100% ionic, has suggested that bond ionicity is a critical parameter governing which environments will enhance crack growth in brittle materials. Our continuing investigation of the effects of environment on the fracture of brittle materials has focused on two materials: single crystals of Si and GaAs. These materials were chosen because they represent a wide range of ionicity, Si being totally covalent and GaAs being approximately 70% ionic.

Experimental Procedure:

GaAs:

Last year, preliminary work on undoped, LEC GaAs single crystals qualitatively showed that water and methanol enhanced crack growth. However, due to large residual stresses in the materials, no quantitative results could be obtained. This year, we used Si doped, Bridgeman grown GaAs single crystals. In contrast with x-ray topographs of the LEC wafers, the Si-doped Bridgeman wafers displayed uniform curvature but little in terms of random strain patterns or incipient cracks. The crack behavior was correspondingly better behaved. Both indentation and applied moment double cantilever beam (DCB) experiments were conducted in inert as well as reactive environments. DCB specimens ≈12.5 mm wide were cleaved from the GaAs wafers, which were oriented in the 100 plane. Cracks along the 110 cleavage planes were initiated in the specimens by pressing a diamond indentor into one end of the specimens at loads of 10N. The precracked specimens were cemented to aluminum arms and placed in an environmental chamber. Crack lengths were measured through an optical microscope containing a filar eyepiece. Cracks were propagated under dead weight loading conditions and velocity data were obtained as a function of load in various environments.

Indentation cracks were introduced using a Vickers indenter at a load of 5N. Measurements of indentation crack length were made as a function of time after indentation and as a function of position on the GaAs wafers. For environmental studies, the indentation was made through the environment into the specimen. Crack length measurements were begun within 15 seconds after indentation, rather than the 45 seconds previously required, providing greater sensitivity to environmental effects on crack growth.

Silicon:

12.5x1x≈25 mm specimens were machined at NBS from a single boule of silicon. DCB specimens were oriented, using x-ray diffraction patterns, for crack propagation along 111 cleavage planes. Cracks were initiated by the same procedure as outlined above for GaAs. DCB and indentation measurements were made on the specimens.

RESULTS

GaAs

The following environments were tested with GaAs: water, methanol, acetonitrile, and oil. Water and methanol are both a Lewis acid and a Lewis base and both environments enhance crack growth in vitreous silica. Acetonitrile is a polar environment which does not affect crack growth in silica but does do so in the totally ionic MgF_2. Oil, an inert environment, was used as a baseline check. Water, methanol, and acetonitrile all enhanced crack growth in GaAs. In agreement with previous work, no crack growth was observed in oil. The N-values of GaAs in methanol obtained from both DCB experiments and indentation experiments on the same wafers were in agreement, as shown in Table I:

Table I: N-values for DCB and indentation experiments in GaAs

Environment	N_{DCB}	$N_{indentation}$
water	34	41
acetonitrile	44	45
methanol	73	51
oil	too large to measure	

The N-values in Table I derive from the empirical crack growth expression $V = V_0(K_I/K_{Ic})^N$, where V is the crack tip velocity, K_I is the stress intensity factor, K_{Ic} is the critical stress intensity factor, and V0 is a proportionality factor. Figure 1 plots the crack growth data for the GaAs in these three environments. An interesting feature of Figure 1, suggested by Table I, is that acetonitrile increases crack growth less than water but more than methanol, which is the least effective of the three environments. During a control test of the indentation technique, indentations made in oil show no sign of enhanced crack growth. This point is particularly important since it suggests that the presence of water impurities in an environment will not be confused with a bulk environment which enhances crack growth.

Finally, consistant with last year's results on the LEC specimens, DCB experiments on the Bridgeman specimens in ammonia gas did not evidence environmentally enhanced crack growth.

Silicon:

During preliminary work delayed failure was observed in Si specimens which were being prepared for DCB experiments. The failures occurred during precracking of the specimens after the diamond indentor was loaded onto the surface. At periods of time ranging from several seconds to several minutes, cracks would pop into the specimens. As a result, experiments were conducted

on Si DCB specimens to try to detect slow crack growth. Specimens were placed into a solution of 1M HCl which included 1%-1.5% HF. This solution was chosen because HCl attacks Si, while HF attacks SiO_2, which is expected to form along the crack walls and at the crack tip. Several specimens were used for the experiments and were loaded until failure without slow crack growth being observed. Two specimens were loaded to within 95% and 98%, respectively, of failure and left for several weeks. Again, no crack growth was observed. After the experiments, all of the specimens were seen to be highly corroded, indicating that the environments did attack the specimen surfaces.

Indentation experiments on the same specimens suggested that slow crack growth might occur in this environment but that the N value would be very large.

CONCLUSIONS

Table II summarizes the known effects of environmental effects on crack growth in Si, SiO_2, GaAs, and MgF_2:

Table II

	Ionicity(%)	Acid	Water	Methanol	Acetonitrile	Oil
Si	0	Maybe	No	No	No	No
SiO_2	≈70	Yes	Yes	Yes	No	No
GaAs	≈70	?	Yes	Yes	Yes	No
MgF_2	100	?	Yes	?	Yes	No

Silicon, which is totally covalent, exhibits no clear environmental enhanced crack growth. In fact, cracks in water appear to grow less than in oil. In the acid solution, there might be some slow crack growth, but the slope is extremely steep. SiO_2, ≈70% ionic, requires an environment which acts both as a base and an acid for environmental effects to be important. GaAs has about the same ionicity as SiO_2 and, from the environments tested to date, displays slow crack growth in water and methanol; environments which cause slow crack growth in SiO_2. However, GaAs also experiences slow crack growth in acetonitrile, an environment which does not cause similar behavior in SiO_2 but does in MgF_2, a material which is 100% ionic. In fact, acetonitrile appears to be more effective than methanol at enhancing crack growth in GaAs. On the other hand, GaAs does not exhibit slow crack growth in ammonia gas, while SiO_2 does. Therefore, an explanation based solely in terms of bond ionicity without regard to the actual bond structures of the materials as a function of applied stresses appears too simplistic to predict which environments will enhance crack growth in a particular material.

(2) Capacitors

The primary effort on capacitor ceramics during this past year was directed toward establishing the relationship between dielectric aging and the fracture strength of the material. Preliminary data (1) obtained on a Z5U material which had been heat treated under different conditions showed a correlation between the rate of dielectric aging and the decrease with aging time of the stress needed to fracture specimens from small indentation induced cracks. In contrast, the strength of specimens indented with a load of 5N

which would produce a larger crack, was constant or perhaps increased slightly with aging time. In order to confirm this behavior, further data was taken on the higher aging rate Z5U material. The specimens were heated to 150°C, cooled to room temperature, and allowed to age under ambient conditions. After various periods of time specimens were indented at a load of 0.3N and fractured in fluorinert at a temperature of ≈3°C. This lower test temperature was chosen in order to be far below the Curie point in this material, so that any effects of internal stresses generated by the phase transformation would be maximized. The strength versus aging time data shown in Figure 2 shows the same trend as that previously obtained, namely a distinct decrease with aging time. Again, the strength of specimens indented at a 5N load remained constant. The decrease in strength has been hypothesized to be due to the redistribution of the internal stresses in the material with the nucleation of additional 90° domains. The fractographs shown in Figure 3 suggest a greater crack-domain interaction in the material aged for the longer time. Both 0.3N and 5N fracture data obtained at 3°C, as well as the capacitance itself is shown as a function of aging time for an X7R ceramic in Figure 4. The rate of strength decrease roughly parallels the measured decrease in capacitance in this material.

In addition, during this past year a thermal wave analysis technique was used to determine the thermal diffusivity of various capacitor compositions. The results are described in an accompanying preprint of a paper to be published in Advances in Ceramics. The ultimate use of this data is in the prediction of thermal shock resistance of capacitor ceramics.

References

1. T. L. Baker and S. W. Freiman, Mat. Res. Soc. Symp., 72, 81-90 (1986)

Figures

Figure 1 Crack velocity - K_I plots for GaAs tested in various environments. The data for water and acetonitrile suggest the possibility of a stress corrosion limit.

Figure 2 Indentation strength (.3N) measured at 3°C as a function of aging time at room temperature for a ZSU ceramic. ▲ Run 1; • Run 2.

Figure 3 Scanning electron micrographs of fracture surfaces of ZSU ceramic aged for 4 and 528 hours. The greater incidence of crack-twin interactions in the longer aged material is indicative of the nucleation of 90° domains.

Figure 4 Indentation strength (.3N and 5N) and capacitance of an X7R ceramic as a function of aging time at room temperature. The strengths were measured at 3°C, the capacitance at ambient temperature. The different symbols in the capacitance plot represent three separate specimens. Curve for the 0.3N strengths represents the best fit to the data.

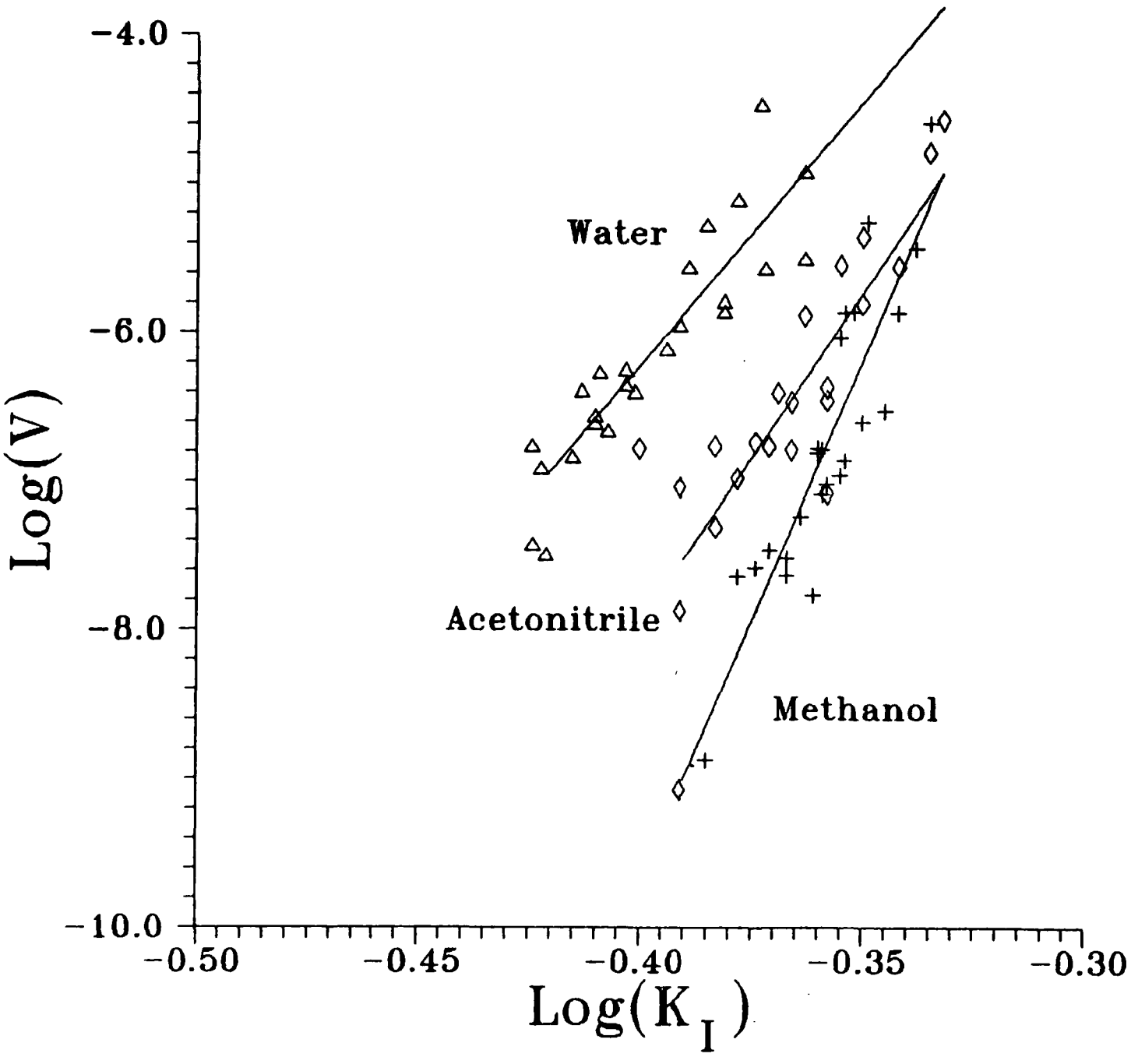
-4.0
-6.0
-8.0
-10.0
Log(V)
-0.50
-0.45
-0.40
-0.35
-0.30
Log(K_I)
Water
Acetonitrile
Methanol

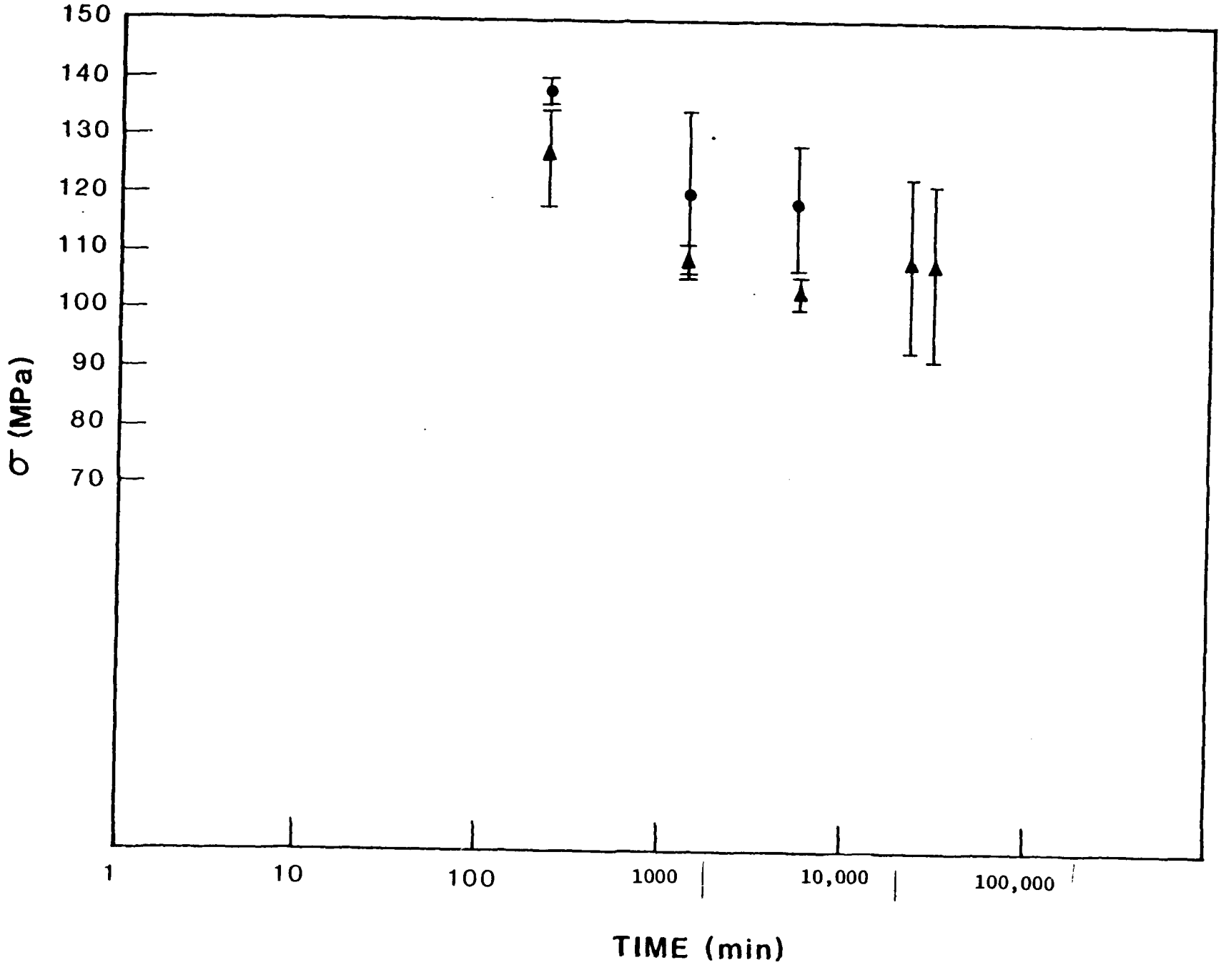
150
140
130
120
110
100
90
80
70
σ (MPa)
1
10
100
1000
10,000
100,000
TIME (min)

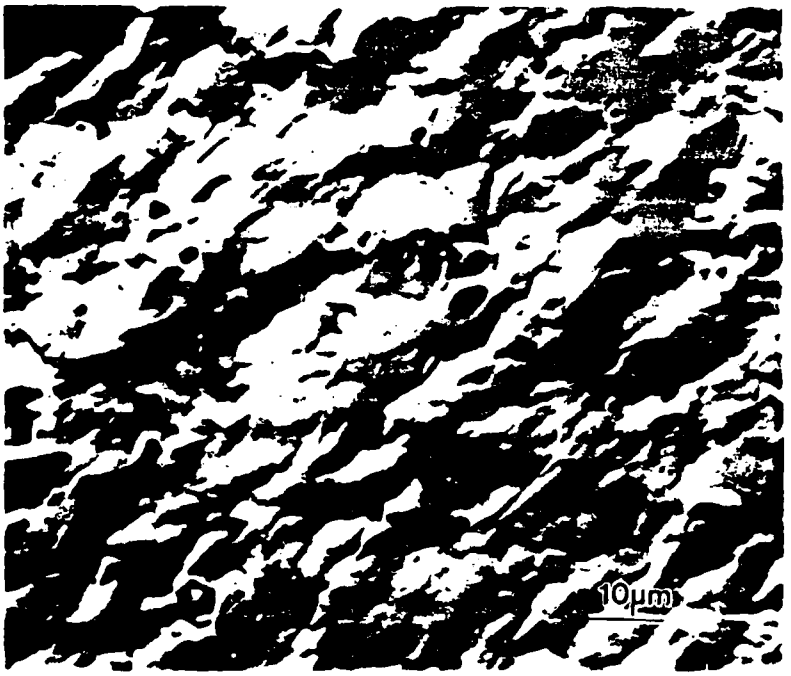

Z5U - Aging Time, 4 hours

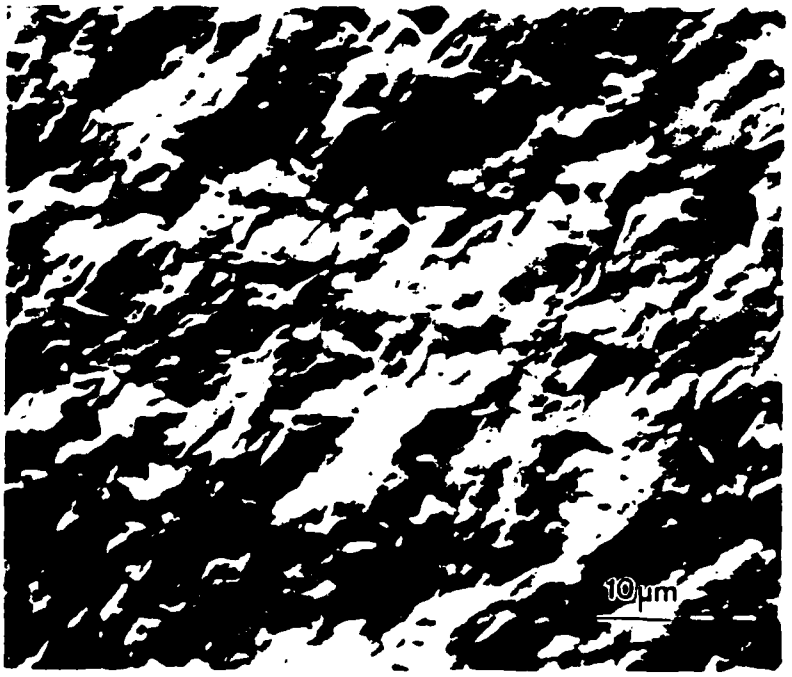

Z5U - Aging Time, 528 hours

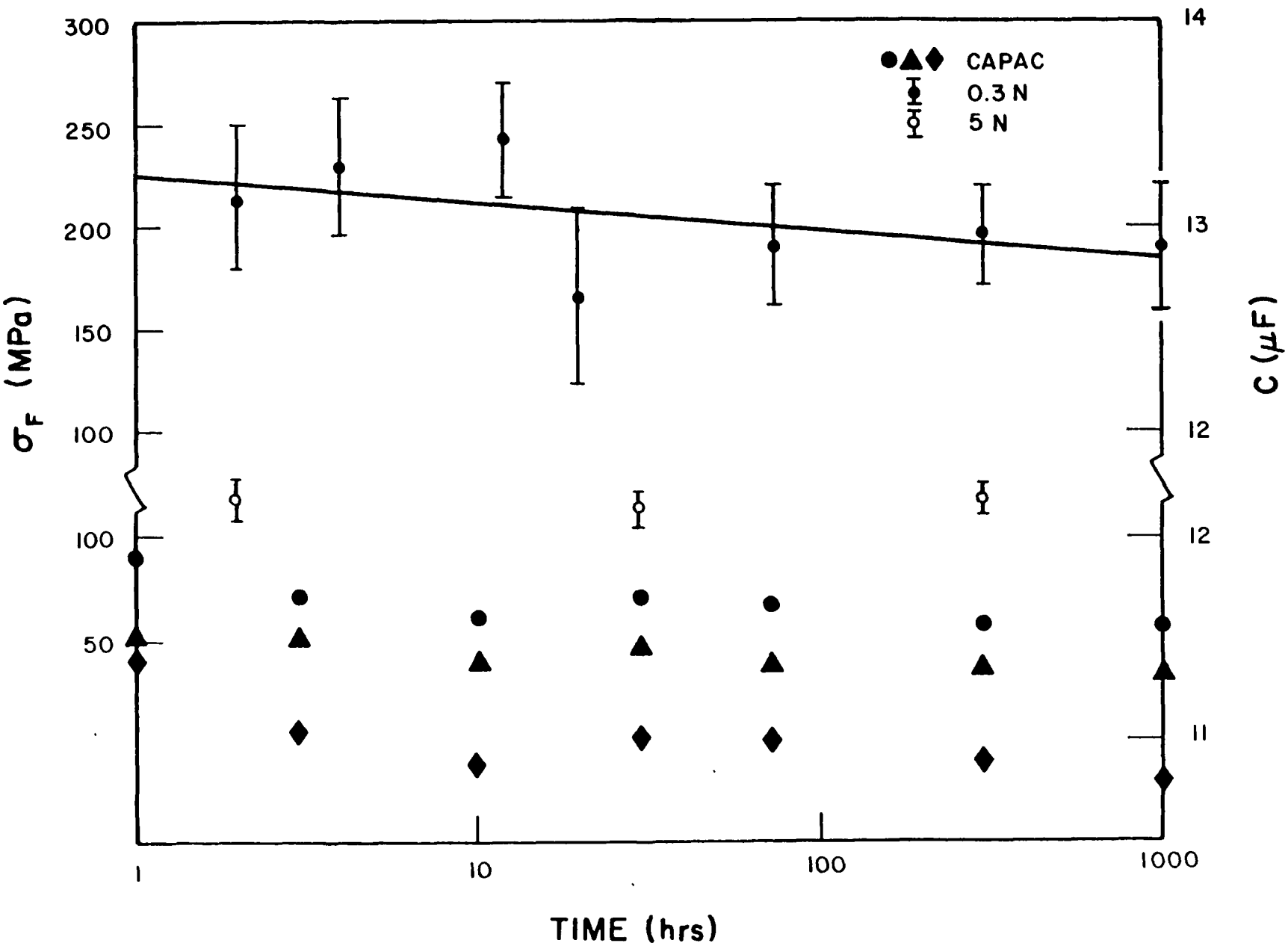
300
250
200
150
100
100
50
14
13
12
12
11
σ_F (MPa)
C (μF)
CAPAC
0.3 N
5 N
1
10
100
1000
TIME (hrs)

Effects of Crystal Bonding on Brittle Fracture

G.S. White, S.W. Freiman, E.R. Fuller, Jr., and T.L. Baker

INTRODUCTION

Compounds from the IV, III-V, and II-VI columns of the Periodic Table form a series of materials having essentially the same crystal structure but whose atomic bonds possess differing proportions of ionic and covalent character. Such a series of materials provides us with the opportunity to investigate how bond ionicity affects brittle fracture while minimizing possible complicating contributions resulting from changes in atomic symmetry. Two aspects of brittle fracture in these materials will be considered in this paper. The first part of the paper discusses the calculation and measurement of the fracture energy for single crystal compounds. Throughout this paper, we assume an equivalence between fracture energy, meaning the energy required to grow a crack in the absence of environmental effects, and surface energy, the energy required to separate two planes of atoms to infinity. Implicit in this assumption of equivalence is the assumption that surface relaxation effects can be ignored. An indentation technique was used to measure values of the fracture energy, γ, which were then compared with those calculated using a model developed by previous investigators[1,2,3].

The second portion of the paper concerns the determination of those environments which enhance crack propagation. Studies have demonstrated that certain chemical environments increase crack growth rates in some brittle materials well above the rates observed in inert environments[4,5]. Recent work[6] has shown that the environments that enhance fracture appear to vary depending on the types of bonds fractured. For example[6], acetonitrile, which

does not enhance crack growth in mostly covalent (≈ 70%) vitreous silica, does do so in MgF_2, which is ≈100% ionically bound. On the other hand, ammonia vapor, which is an ineffective crack growth agent for MgF_2, enhances fracture in vitreous silica. This work led to the hypothesis that variations in the ionicity of the chemical bond in the solid lead to different crack growth mechanisms and, hence, to variations in which environments would affect crack propagation. However, this hypothesis is difficult to evaluate because, in the previous work, other material parameters such as crystal structure have not been held constant. The materials used in this work were chosen to address this difficulty. For the fracture energy determination, the compounds studied were those that crystallize in the diamond cubic structure and its bi-molecular equivalent, the cubic sphalerite structure. In addition, two materials, CdS and CdSe, which have hexagonal rather than cubic symmetry, were included because their nearest neighbor symmetries were the same as those of the sphalerite materials. For the investigation of environmental effects on fracture, other materials such as MgF_2 were included in order both to expand the range of bond ionicity to nearly 1.0 as well as to compare results with those of the previous investigation.

EXPERIMENTAL PROCEDURE

Materials

Single crystal specimens of Si, GaAs, GaP, ZnTe, ZnS, ZnSe, and MgF_2 were obtained from a number of sources and ranged in size from 4 to 36 mm^2. The crack syscems which were investigated ranged in size from about 50 μm to 150 μm and were separated from neighboring cracks by at least that distance. At least 5 crack systems were measured for each data point.

Determination of the crack planes was made by x-ray diffraction for Si (111) and GaAs (110), for which sizable specimens were available. For the other materials, we assumed that the cracks propagated along the easiest cleavage planes, as was observed in the cases of Si and GaAs.

Indentation Technique

The indentation-crack length technique, as described by Anstis et al.[7], was used for both fracture and environmental effects measurements. With a standard hardness machine[a], a Vicker's diamond pyramid was pressed into the sample to generate a deformation zone with fourfold symmetry in the material. This deformation zone acted as a wedge to drive cracks nucleated during or shortly after the indentation procedure. The resulting crack system consisted of a set of cracks emitted radially about the indentation impression and a set of subsurface lateral cracks which began parallel to the specimen surface and curved upward to intersect it. The radial crack lengths were measured in an optical microscope. The magnitude of the indentation load was chosen to produce clearly defined radial cracks while minimizing lateral cracking. The specimens were oriented to force at least one radial crack to emanate from the corner of the impression made by the indenter. Because most specimens were indented on a plane of trigonal symmetry, there generally were three cracks radiating from the impression, only one of which came from a corner of the indentation impression; in these cases, measurements were made only on that one crack.

To determine effects of environment on crack growth in the materials, crack length measurements were made in different liquid environments by indenting the specimen through the liquid, then covering the indentation with a glass

cover slide during the microscopic measurements of the crack length as a function of time. For the fracture energy determinations, an "inert", silicone based diffusion pump oil[b], which had been dried for 16 hours in air at 125C and stored in a desiccator, was used. Comparisons among environments were made by measuring crack lengths at the same elapsed time after indentation. Because of the time required to transfer the specimen between indenter and microscope, an interval of 30 to 45 seconds between the indentation process and the crack length measurement was maintained; this interval was constant for each material.

To determine that the driving force for the crack systems was independent of changes in environment, the indentation impression, the source of the driving force, was measured in each environment. Within experimental uncertainty, the impression size was independent of environment. Therefore, we assumed that the crack system for a given material experienced the same driving forces regardless of the environment in which the indentation was made.

THEORY

Fracture Energy

Indentation Calculations

The fracture energy, γ, is related to the cohesive forces between the planes of atoms. At equilibrium, the cohesive force is equal to the driving force at the tip of a crack which, in turn, can be represented in terms of linear elastic fracture mechanics by a stress intensity, K_I, at the crack tip[7]:

$$K_I = \chi P/c^{3/2} \tag{1}$$

where

$$\chi = \Omega(E/H)^{1/2} \tag{2}$$

P is the indentation load, c is the crack length, Ω is an empirically determined constant ($\approx$.016), E is Young's modulus, and H is the material hardness. Although the formalism developed for evaluating the stress intensity factor, K_I, using the indentation technique, assumes a crack system with fourfold symmetry, resulting from the symmetry of the diamond pyramid pressed into an isotropic material, calculations have been made[8] which show that the value of K_I changes by less than 10% when a three crack system is present. This change is well within the uncertainty of our measurements. Nevertheless, because equation 1 was derived for isotropic materials, some modification for use in highly directional materials such as single crystals

is required. Specifically, the value of $\underline{E}$ used in eqn. 2 was obtained from the angularly dependent Young's modulus[9] averaged over all angles:

$$\underline{E} = (1/4\pi) \int_0^{\pi} \int_0^{2\pi} E(\theta,\Phi)\cos\theta d\theta d\Phi \qquad (4)$$

This value was used because the residual driving force from the indentation is distributed over the volume of the indentation compression zone and is not localized to the crack plane. The fracture energy is now evaluated, using the results of Sih et al.[10] for a cubic material:

$$\gamma = K_{Ic}^2 (s_{11}/2^{1/2})[1+(2s_{12} + s_{44})/2s_{11}]^{1/2}/2 \qquad (5a)$$

and for a hexagonal material, i.e. CdS and CdSe:

$$\gamma = K_I{}^c{}_2 s_{11}/2 \qquad (5b)$$

In eqn. 5a and 5b, the s_{ij} are the compliances and were evaluated by inverting the matrix for the stiffness constants, c_{ij}, shown in Table I.

Model Calculation

For a reversible, thermodynamic process, the fracture energy of a material is equal to the energy needed to form two new surfaces, assuming no surface relaxation. In determining γ by a fracture experiment, we must therefore assume that no energy is consumed by inelastic processes such as dislocation

generation. We have used a continuum model to describe the restoring force between two planes of atoms as an average force/unit area, σ. Consistent with previous authors[1,2], we have chosen as our model σ, $\sigma(\delta/\delta_c) = \sigma_m \sin(\pi\delta/\delta_c)$, where δ is the displacement of the atom planes from their equilibrium separation, d. γ was determined in the following expression:

$$2\gamma = \sigma_m \int_0^{\delta_c} \sin(\pi\delta/\delta_c) \tag{6}$$

In this expression, δ_c is the value of δ for which the restoring force is 0 and, more importantly, beyond which an increase in δ does not change γ. To obtain a numerical value for γ, the value of δ_c must be known. In the absence of a method for rigorously evaluating δ_c, we follow the lead of previous workers[1,2] and arbitrarily choose $\delta_c = d$, corresponding to a zero restoring force for $\delta/\delta_c = \delta/d = 1$, e.g. to a strain of 100% at bond failure. To evaluate σ_m, we recognize that, for small δ, the restoring force/unit area, σ, is linear: i.e.

$$\left.\frac{d\sigma}{d\delta}\right|_{\delta=0} = \sigma_m \left.\frac{d(\pi\delta/d)}{d\delta}\right|_{\delta=0} = \frac{\sigma_m \pi}{d} \tag{7}$$

However,

$$\left.\frac{d\sigma}{d\delta}\right|_{\delta=0} = \frac{1}{d}\left.\frac{d\sigma}{d\epsilon}\right|_{\epsilon=0} = \frac{E}{d} \tag{8}$$

where E is Young's modulus and ϵ is the strain. Therefore,

$$\sigma_m = E/\pi \tag{9}$$

giving the surface energy, γ:

$$\gamma = \frac{Ed}{\pi^2} \tag{10}$$

Normalized γ and K_I

The purpose of studying iso-structural specimens (within nearest-neighbor distances) is to minimize effects on γ resulting from changes in material parameters other than bond ionicity. However, there remains one parameter which affects γ and changes from specimen to specimen: the lattice spacing as influenced by the varying ionic radii in these compounds. To normalize γ for the influence of ionic size, we assume γ can be written as $\gamma = \gamma_0 \gamma^*$ where γ_0 contains the ionic radius component of the fracture energy and γ^* contains remaining components such as bond symmetry and ionicity. Further, we assume, on dimensional grounds, that γ_0 can be expressed as:

$$\gamma_0 = e^2/d^3 \tag{11}$$

This normalization is analogous to that used by Keyes[19], e^2/d^4, to normalize elastic moduli. Using this normalization factor, we can compare γ^* of the different compounds as a function of bond ionicity without complications induced by variations in ionic sizes.

Environmental Crack Growth Enhancement

The most important parameter in environmental crack growth studies is the degree to which the propagation velocity, $V(K_I)$, of a crack in a stressed specimen is increased above that observed in inert environments. To obtain this information from indentation experiments, it is necessary to measure the crack length, c, as a function of time, t, after indentation. Unfortunately,

experimental constraints make measurements of this type impractical for many environments (see Appendix I). However, at least a qualitative determination of those environments which will enhance crack propagation can be made using indentation techniques; specifically, a measurement of c_1/c_2, where c_1 is determined in the environment of interest and c2 is measured in an inert environment, will always be greater than 1 if environment 1 enhances crack growth.

RESULTS AND DISCUSSION

Fracture Energy

Table II lists the calculated and measured values of γ and γ^* for the crystals studied. Figure 3 plots the values of γ^* as a function of f_i, where f_i is the bond ionicity determined from the Phillips-Van Vechten ionicity scale[20,21]; included in the figure are fracture energy data for Si[3c,22], GaAs[23], and ZnSe[24] obtained by double cantilever beam tests. Three separate ideas shown in Figure 3 are discussed below.

The first point is that values of γ^* determined by the double cantilever beam (DCB) technique in previous studies agree very well with those obtained through indentation measurements. This agreement confirms that the indentation technique can be used to determine γ in single crystals even though the elastic strain pattern around the indentation is highly non-isotropic.

The second point to note in Figure 3 is the close agreement between the experimentally measured and the calculated values of γ^*. The values of γ^* determined experimentally and analytically lie within about 50% of each other

and exhibit no systematic trend between experimental and calculated values. This result is quite remarkable when it is remembered that the only adjustable parameter in the model, the strain at fracture, was arbitrarily set at 100% and that the calculation of γ included very general assumptions. Similar agreements between calculated and measured values of γ have been obtained on other materials[25]. The agreement suggests that the simplistic model of a sinusoidal force law does in fact give reasonable values for γ. The actual physical parameters of the individual materials, E and d, place constraints upon possible values of γ limiting them to physically reasonable values. For example, the values of E used to determine γ (or γ^*) in Table II were directionally dependent; for Si, Ge, and C, E was determined across the (111) cleavage plane and, for the other materials, across the (110) cleavage plane. The agreement between the experimentally determined values of γ and the model suggest that more precise estimates of the force law may be expected to improve the values of γ but not to alter them drastically.

The third point to notice about the data in Figure 3 is the trend of γ^* toward 0 as the ionicity of the bonds increases. While there is some scatter in the data, a line drawn through the data points would reach 0 for an ionicity of about 0.8. It may be significant that, for $f_i > 0.8$, the diamond structure is no longer stable. Similar observations were made by Martin[26,27] for elastic properties of these materials.

Environmental Crack Growth Enhancement

Figure 4 shows the results of indentation crack length measurements made on Si, GaAs, ZnS, and MgF_2 in dry oil, heptane, acetonitrile, and water. The vertical axis plots the crack length measured in the specified environment normalized by the crack length (for the same load and delay time) measured in

oil, c/c_o. Dry diffusion pump oil was used to provide an inert environment. As discussed previously, environments in which the cracks grow more readily than in oil are expected to give values of $c/c_o>1$. The dashed line in Figure 4 marks the value of $c/c_o=1.0$ and the shaded region represents uncertainty in the measurements. In oil, $c/c_o=1$, by definition.

Heptane was chosen to determine if water impurities in the environment would invalidate the test procedure; heptane itself is known not to enhance crack growth in MgF_2 but the water impurities in it (about 30% relative humidity) do lead to crack growth in glasses. The fact that c/c_o for MgF_2 in heptane was indistinguishable from that in oil suggests that water impurities in an environment will not produce significant crack growth, so that this indentation procedure can be used to determine if the bulk environment will enhance crack growth. In heptane, for both Si and MgF_2, $c/c_o=1$ within the uncertainty of the measurement.

Acetonitrile was investigated because it does not enhance crack growth in vitreous silica (about 30% ionic) but does do so in MgF_2 (100% ionic). The results in Figure 4 show that crack growth is enhanced by acetonitrile for all of the materials but Si.

Finally, water was studied because: a) it enhances crack growth in both ionic and partially covalent solids and b) it is present as an impurity in almost every environment. As seen, water also enhanced crack growth in all the materials with the exception of Si. In Si, c/c_o was consistently <1.0 which suggests that water may actually inhibit crack growth relative to oil. This observation was quite unexpected and, currently, we have no explanation for it.

As mentioned previously, hardness measurements were made in all the environments and, within experimental uncertainty, no differences were observed. This suggests that the driving forces for the cracks, resulting from the residual stresses around the indentation impressions, were approximately the same. Therefore, we expect differences in crack lengths to reflect environmental effects on crack propagation itself.

CONCLUSIONS

The work described herein leads us to several conclusions:

1) values of fracture energy measured on single crystals by the indentation crack length technique are in excellent agreement with those determined by conventional fracture mechanics methods;

2) measured values of fracture energy are in surprisingly good agreement with those predicted from a fairly simplistic model;

3) both measured and predicted values of fracture energy decrease with increasing ionicity of the compound;

4) GaAs, ZnS, and MgF_2 are susceptible to environmentally enhanced crack growth, but no change in mechanism with ionic/covalent bond ratio could be determined.

In addition, the potential and some of the limitations of the indentation technique as a probe for determining fracture energy values as well as environmental effects on fracture have been demonstrated.

Appendix I:

Gupta and Jubb[28] derived the following expression and used it to measure crack growth in soda lime glass:

$$c/c_i = [(3n+2)V_0 t/2c_i]^{2/(3n+2)} \qquad \text{for } t \gg 2c_i/(3n+2)V_0 \qquad (A1)$$

where c_i is the initial crack length after indentation and n and V_0 are empirical parameters in the expression relating crack velocity, i.e. crack extension rate, to K_I:

$$V = V_0 (K_I/K_{Ic})^n \qquad (A2)$$

In eqn. A2, $K_{Ic} = XP/c_i^{3/2}$. Although, in principle, crack growth curves can be obtained through the indentation technique, for large values of n, the technique becomes unreliable, as figure A1 shows. In the figure, equation A1 is plotted for two values of n; n=20 and n=80. The error bars show the resolution limit of our optical microscope ($\approx$ 7 μm) and the vertical dashed line shows the shortest time to move the specimen from the hardness tester to the microscope ($\approx$ 30 s). It is important to note that the time axis is logarithmic, so that changes in either the delay time or the length of time over which observations are made must be large to have much effect. All crack growth information for times to the left of the dashed line or for crack growth increments smaller than the error bars is lost. For the two cases in the figure, crack extension for a material having a value of n=20 could be determined with reasonable precision, but for a material whose n=80 crack extension with time is completely lost within the resolution of the

experiment. With our experimental arrangement, crack growth could be observed only in those materials having an n<35.

However, qualitative determinations of the effects of an environment on crack propagation can still be obtained in certain circumstances. The ratio of crack lengths in two environments measured at the same time, t, after indentation can be obtained from eqn. A1:

$$c_1/c_2 = [(1+a_1 t)^{1/\alpha 1}]/[(1+a_2 t)^{1/\alpha 2}] \qquad (A3)$$

In this expression, the subscripts refer to the two environments, the environment being tested (1) and an inert environment (2); α_i and a_i are defined as follows:

$$\alpha_i = (3n_i+2)/2 \qquad (A4)$$

$$a_i = \alpha_i V_i/c_i$$

Figure A2a is a schematic of the log(V) vs K_I curves for two environments, one of which enhances crack propagation (i=1) and the other which is almost inert (i=2). For this situation, eqn A3 (Figure A2b) indicates that for n1>n2, and $V_1 = V_2$, c1/c2 is always >1.

Table I: Stiffness constants used to determine compliances. For cubic symmetry, only c_{11}, c_{12}, and c_{44} are unique. For CdS and CdSe, which are hexagonal, c_{33} and c_{13} are also unique.

Material	c_{11}	c_{12}	c_{44}	c_{33}	c_{13}
C[11]	10.756	1.249	5.758		
Si[12]	1.657	.639	.796		
Ge[13]	1.292	.479	.67		
GaP[14]	1.411	.619	.704		
GaAs[15]	1.190	.538	.595		
GaSb[16]	.884	.403	.432		
ZnS[17]	1.046	.653	.461		
ZnSe[17]	.810	.488	.441		
ZnTe[17]	.713	.407	.312		
CdTe[17]	.535	.369	.199		
CdS[18]	.843	.521	.146	.918	.457
CdSe[17]	.741	.452	.132	.836	.393

Table II: Values of γ and γ^*

Material	γ_{exp} (J/m^2) indent	γ_{exp} (J/m^2) DCB	γ_{calc} (J/m^2)	γ^*_{exp} indent	γ^*_{exp} DCB	γ^*_{calc}
C	-	-	4.7	-	-	.076
Si	2.1	2.1	1.1	.12	.12	.063
Ge	-	-	.96	-	-	.061
GaP	.94	-	1.1	.054	-	.060
GaAs	.87	1.0	.92	.055	.066	.059
GaSb	-	-	.73	-	-	.059
ZnS	1.1	-	.66	.061	-	.037
ZnSe	.66	.60	.60	.043	.039	.039
ZnTe	.56	-	.52	.043	-	.040
CdS	-	-	.21	-	-	.015
CdSe	-	-	.20	-	-	.016
CdTe	-	-	.35	-	-	.033

Figure Captions

1. Schematic drawing of cohesive stress, σ, between two surfaces. At equilibrium ($\sigma = 0$), the atomic planes are a distance d apart. A displacement of δ from equilibrium spacing results in a restoring force/unit area, σ.

2. Plot of the normalized fracture surface energy, γ^*, as a function of bond ionicity for a series of semiconductors from the columns IV, III-V, and II-VI of the periodic table. ○'s are calculated values assuming a sinusoidal surface force between the walls of the crack, □'s are the values obtained through the indentation process. △'s are the values from double cantilever beam tests. γ^* decreases as the bond ionicity increases.

3. Ratio of crack length in an environment, c, to the crack length in oil, c_o, four different environments for Si (0), GaAs (△), ZnS (▽), and MgF_2 (□). The hashed region represents the level of uncertainty in each of the measurements.

A1. Using the expression derived by Gupta and Jubb[28], the crack length, c, is plotted as a function of time, t, after indentation for two values of n, n = 20 and n = 80. The vertical dashed line represents the time after indentation when measurements are begun. The error bars represent the resolution of the optical microscope.

A2. a) A log(V) vs K_I plot for two environments (n_1 and n_2). Environment n_1 enhances crack growth more than environment n_2. The curves intercept at velocity V_0.

b) A plot of the ratio of crack lengths in two environments, measured at the same time after indentation, as a function of the relative n-values in the two environments. For $n_1 < n_2$, the crack length a_1 is always greater than a_2.

REFERENCES

1. E. Orowan, Rep. Prog. Phys. 12 185 (1949).
2. J.J. Gilman, J. of Appl. Phys., 31 [12] 2208 (1960).
3. A. Kelly, Strong Solids (Claredon Press, Oxford, England, 1973), 2nd ed. pp 5,8.
4. S.M. Wiederhorn, J. Am. Cer. Soc., 50 [8] 407 (1967).
5. T.A. Michalske and S.W. Freiman, J. Am. Cer. Soc. 66 [4] 284 (1983).
6. T.A. Michalske, B.C. Bunker, S.W. Freiman, J. Am. Cer. Soc. 69 [10] 721 (1986).
7. G.R. Anstis, P. Chantikul, B.R. Lawn and D.B. Marshall, J. Am. Cer. Soc. 64 [9] 533 (1981).
8. F. Ouchterlony, in Rock Fracture Mechanics, H.P. Rossmanith, ed. (Springer Verlag, New York 1983), pp. 31-68.
9. J.F. Nye, Physical Properties of Solids (Claredon Press, Oxford, England 1979), p.145.
10. G.C. Sih, P.C. Paris, G.R. Irwin, Internt'l J. of Fract. Mech. 1 [1], 189 (1965).
11. H.J. McSkimin, Phys. Rev. 105, 116 (1957).
12. H.J. McSkimin and P. Andreatch, Jr., J. Appl. Phys. 35 #11, 3312-19 (1964).
13. W.P. Mason, "Physical Acoustics and the Properties of Solids," D. Van Nostrand Co. (New York, 1958).
14. R. Weil, Am. Phys. Soc. Bull. 11, 764 (1966).
15. J.R. Drabble, Solid State Comm. 4, 467-68 (1966).
16. H.J. McSkimin, J. Appl. Phys. 39, 4127-8 (1968).
17. Berlincourt, Phys. Rev. 129, 1009 (1963).
18. D. Gerlich, J. Phys. Chem. Solids, 28, 2575 (1967).
19. R.W. Keyes, J. Appl. Phys. 33, 3371 (1962).
20. J.A. Van Vechten, Phys. Rev. 187, 1007 (1969).
21. J.A. Van Vechten, Phys. Rev. B 3 [2], 562 (1971).
22. S.M. Wiederhorn, in Fracture Mechanics of Ceramics, Vol. 2, R.C. Bradt, D.P.H. Hasselman, and F.F. Lange, eds., (Plenum Press, New York 1974) pp. 613,646.
23. S.W. Freiman and G.S. White, unpublished work.
24. R.W. Rice, S.W. Freiman and J.J. Mecholsky, Jr., J. Am. Cer. Soc. 63 [3-4] 129 (1980).
25. P.F. Becher and S.W. Freiman, J. Appl. Phys. 49 [7], (1978).
26. R.M. Martin, Phys. Rev. B1, 4005 (1970).
27. R.M. Martin, Phys. Rev. B6, 4546 (1972).
28. P.K. Gupta and N.J. Jubb, J. Am. Cer. Soc. 64 [8] C-112 (1981).

Footnotes

[a] Zwick 3212 hardness tester. Trade names and companies are identified in order to specify adequately the experimental procedure. In no case does such identification imply that the products are necessarily the best available for the purpose.

[b] Varian Santovac 5 silicone diffusion pump oil. Trade names and companies are identified in order to specify adequately the experimental procedure. In no case does such identification imply that the products are necessarily the best available for the purpose.

[c] The value calculated in ref. 3 was altered by including correction terms in ref. 17.

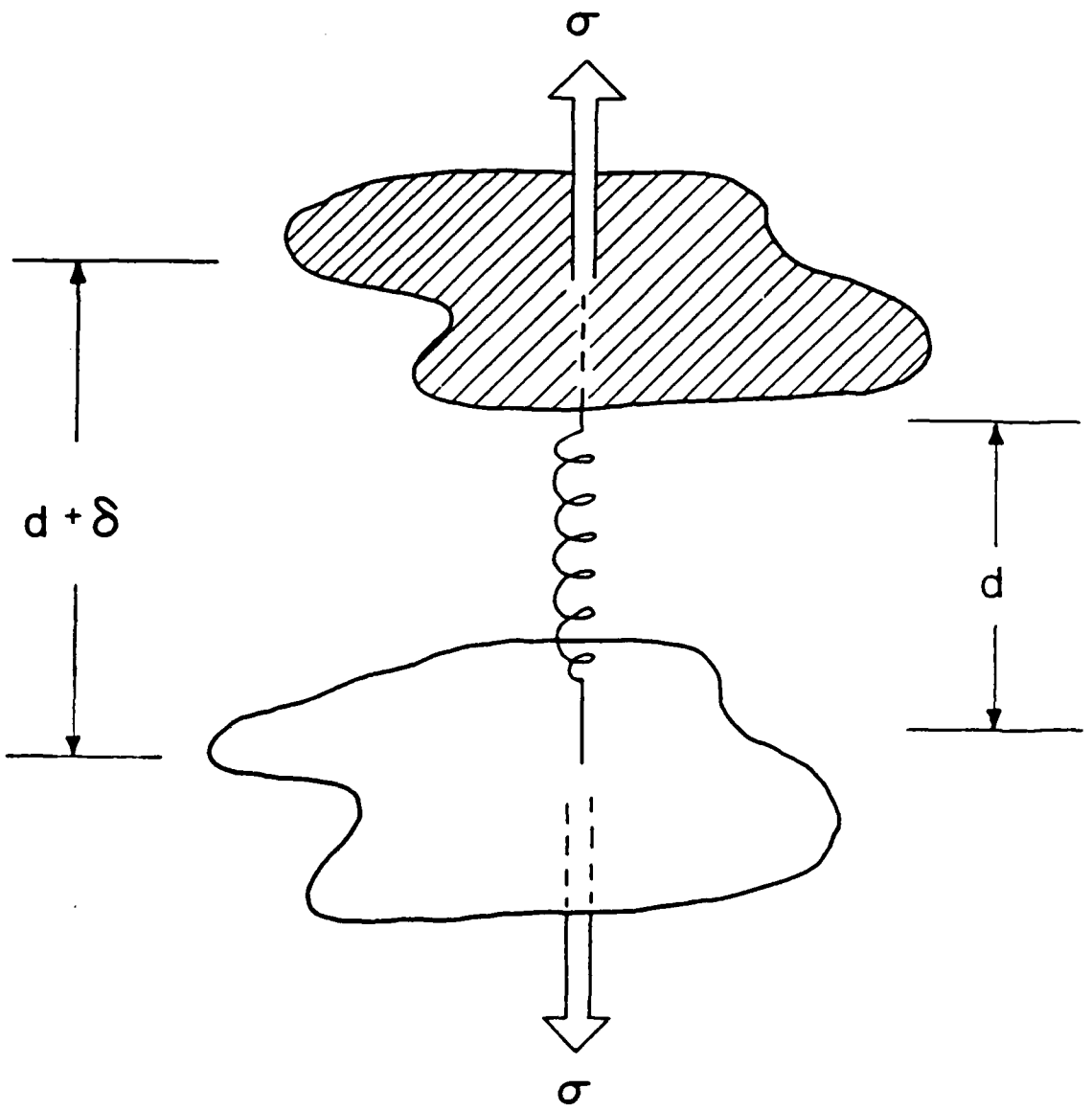
σ
d + δ
d
σ

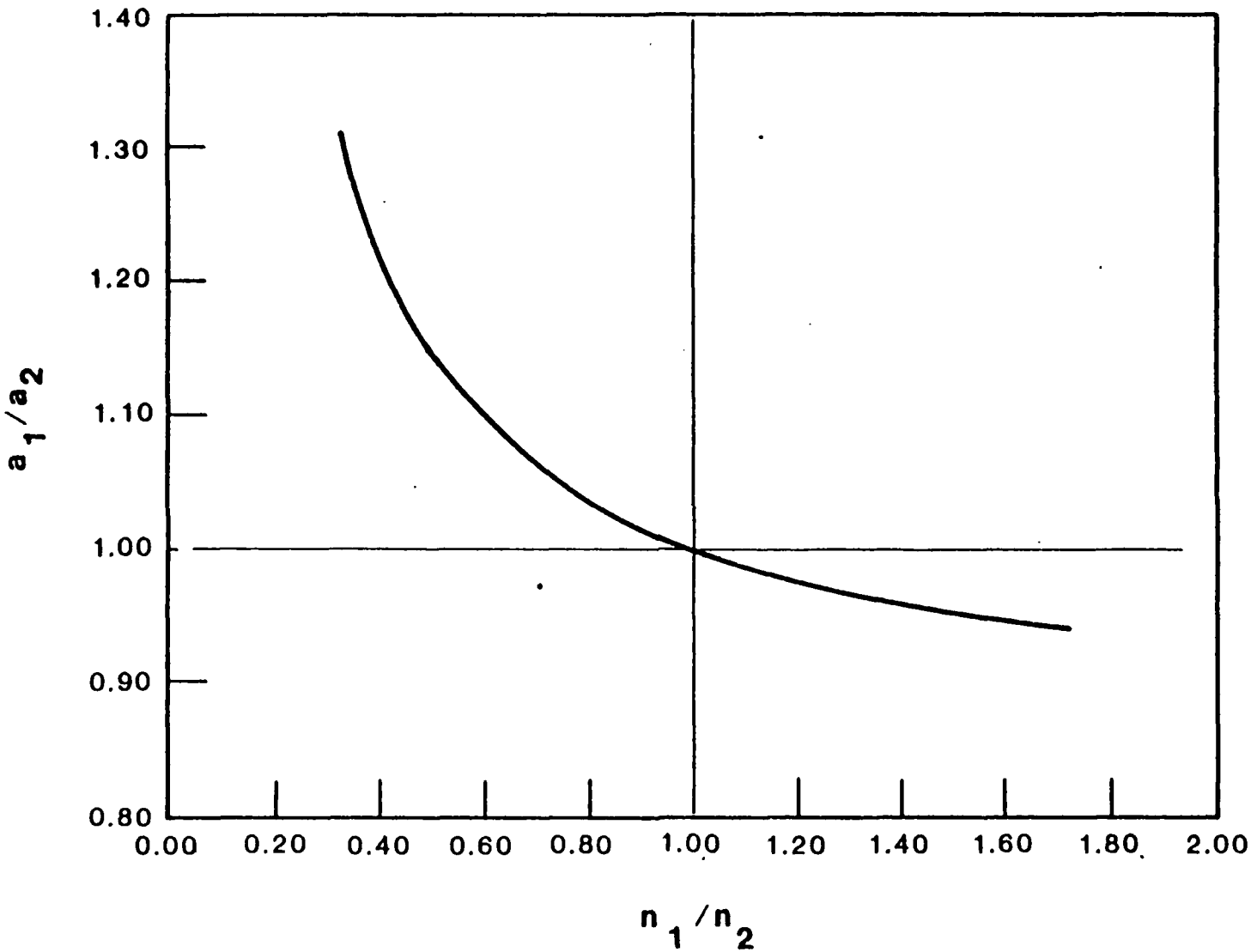
1.40
1.30
1.20
1.10
1.00
0.90
0.80
a_1/a_2
0.00
0.20
0.40
0.60
0.80
1.00
1.20
1.40
1.60
1.80
2.00
n_1/n_2

Fig. 56

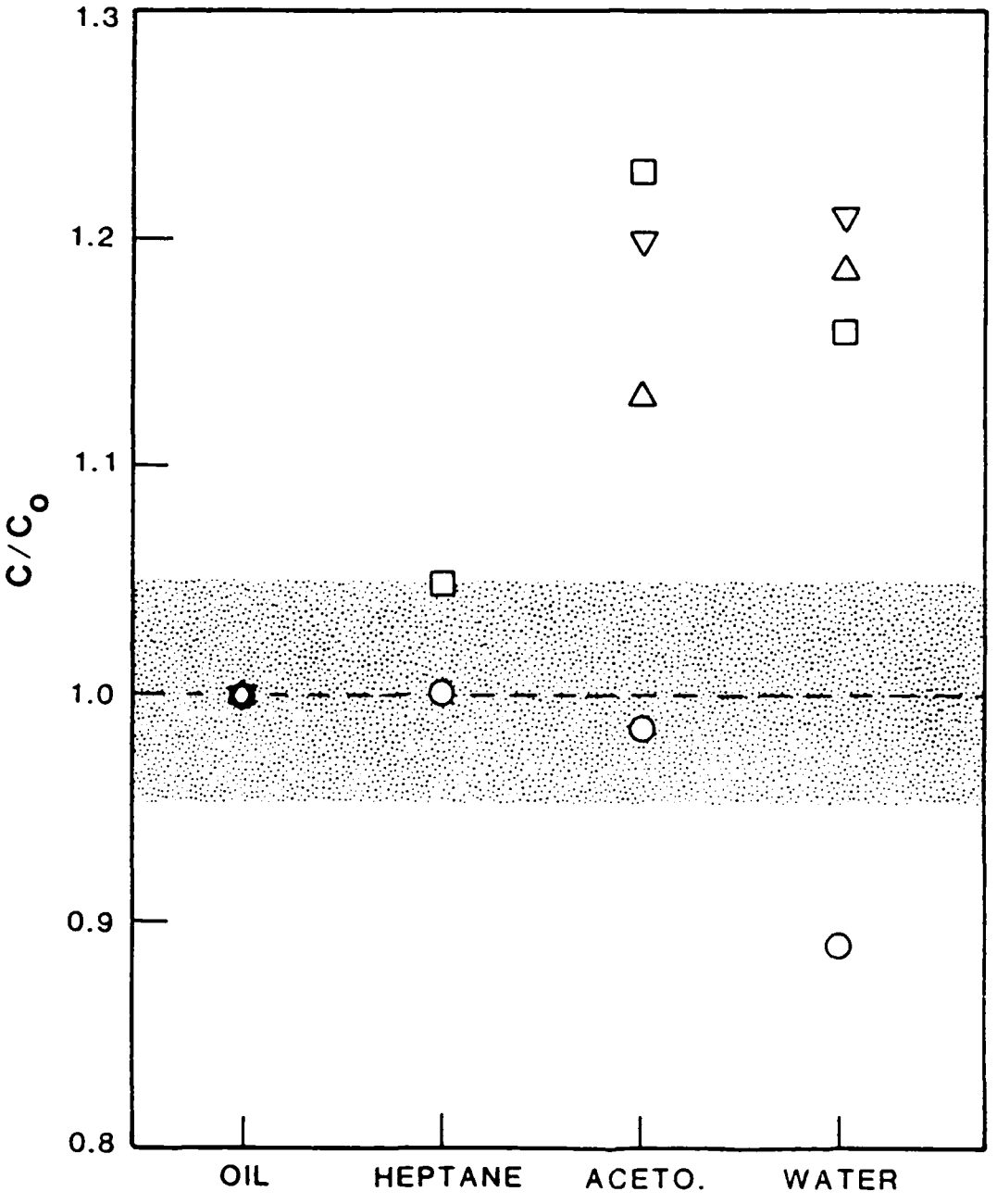

Fig. 3

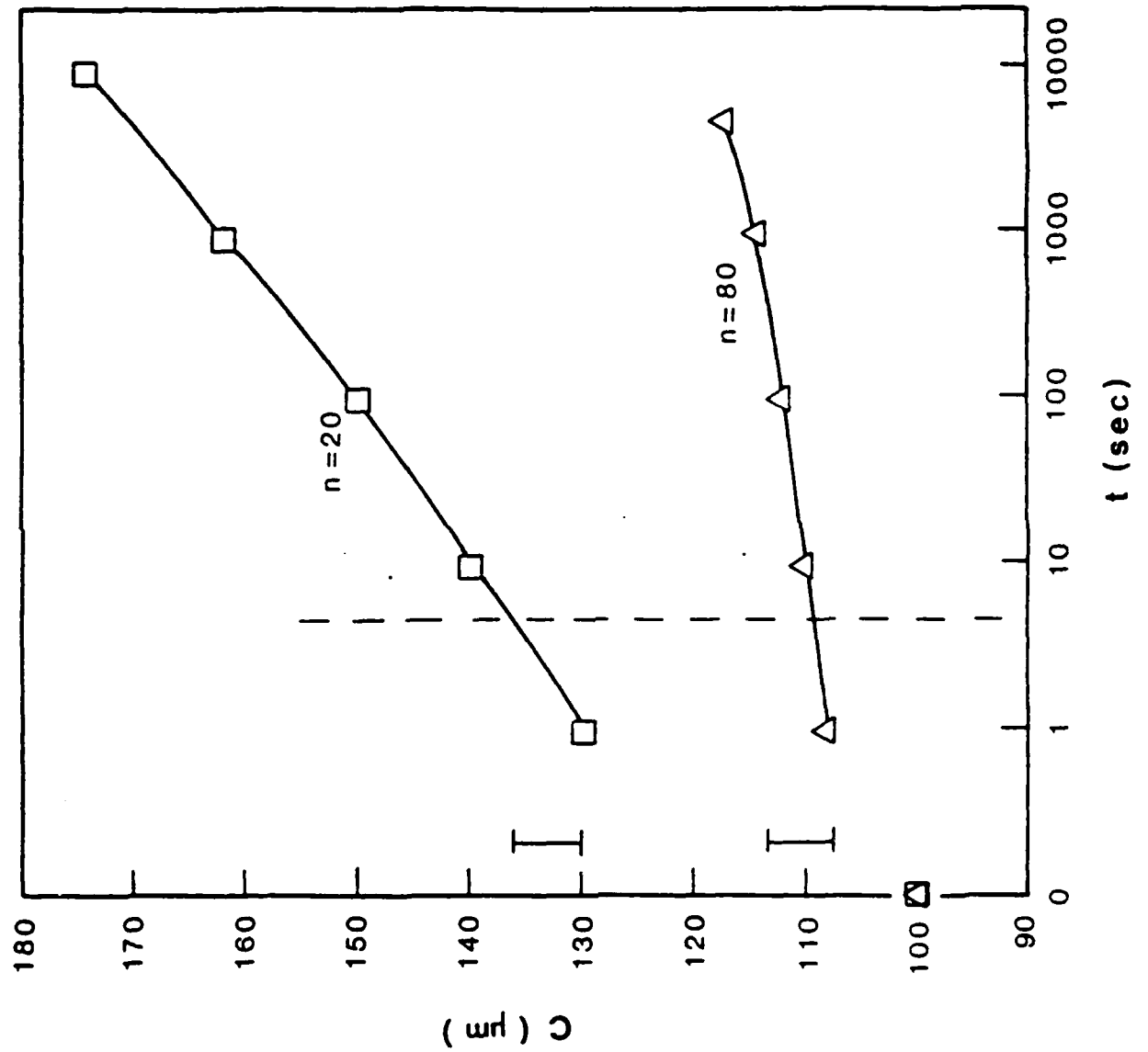
C (μm)
180
170
160
150
140
130
120
110
100
90
0
1
10
100
1000
10000
t (sec)
n=20
n=80

Fig 4

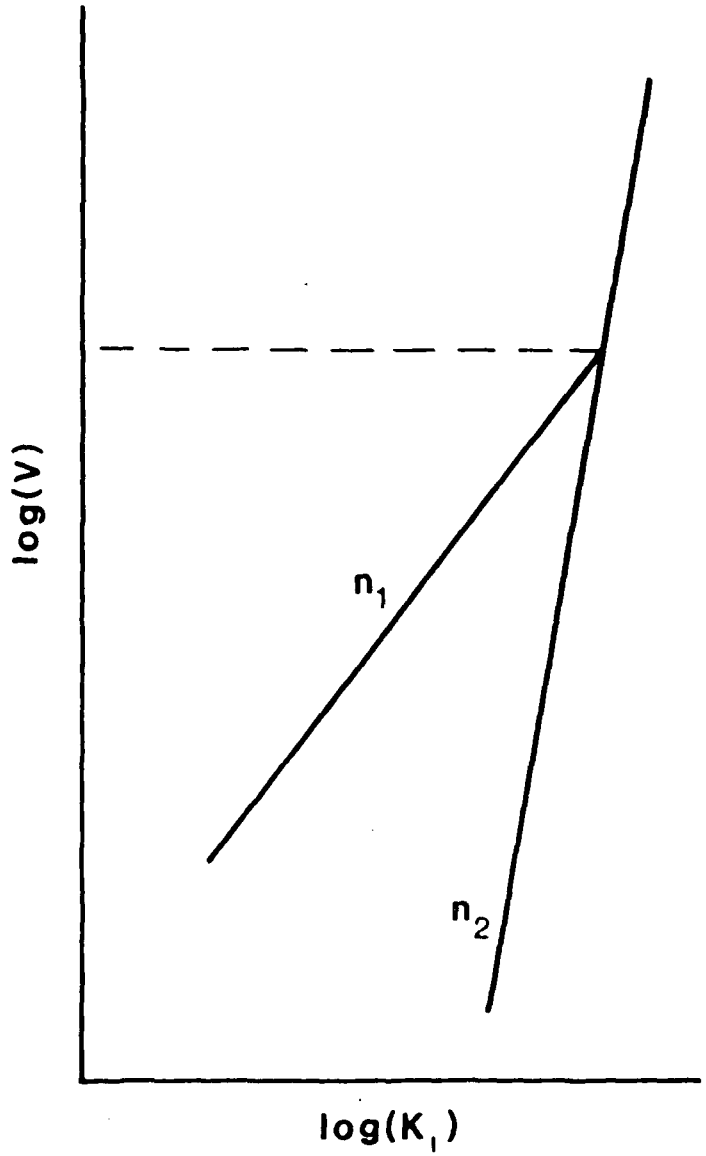

Fig. 5a

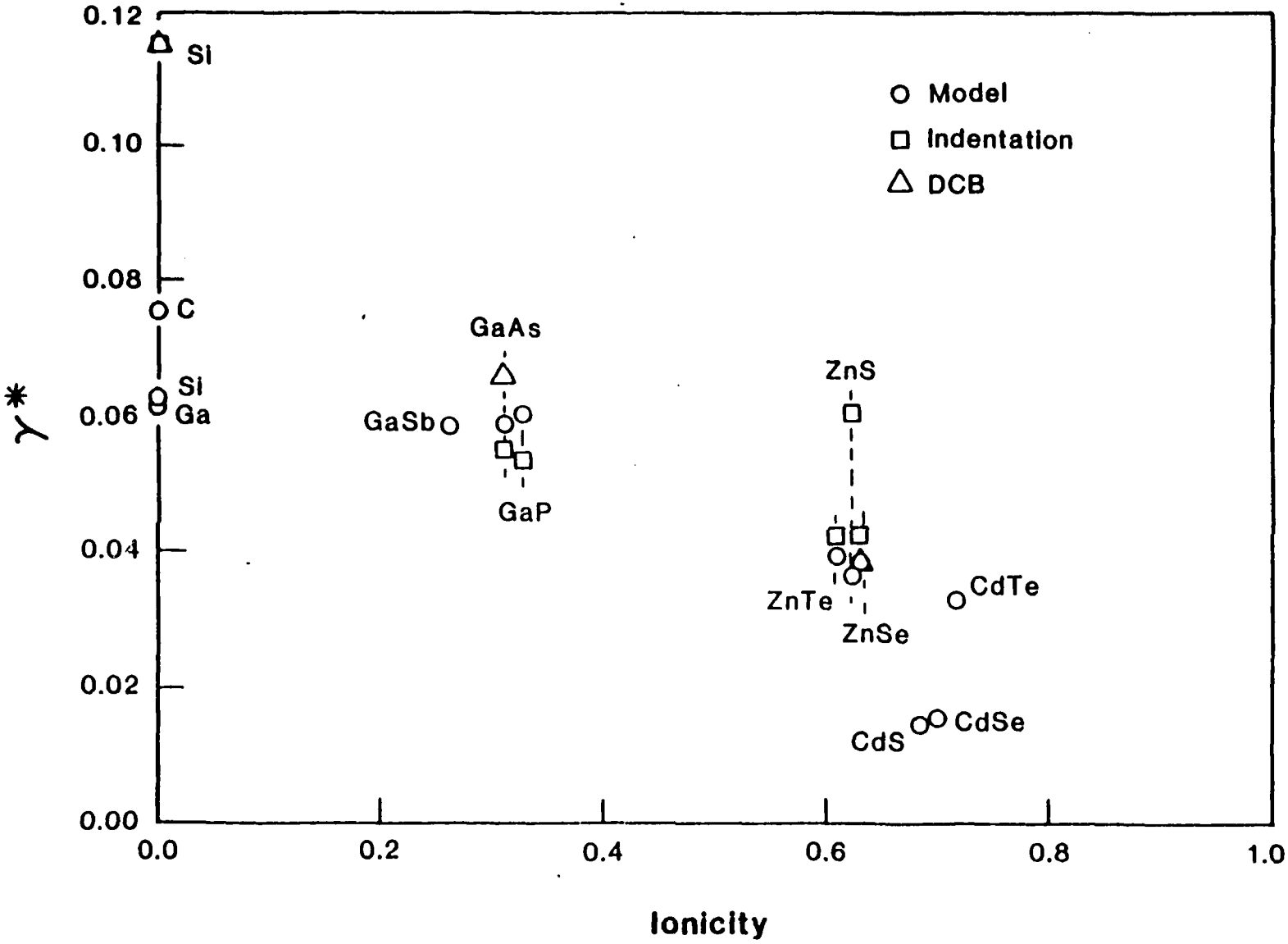
0.12
0.10
0.08
0.06
0.04
0.02
0.00
γ*
Si
C
Si
Ga
GaAs
GaSb
GaP
ZnS
ZnTe
ZnSe
CdTe
CdS
CdSe
Model
Indentation
DCB
0.0
0.2
0.4
0.6
0.8
1.0
Ionicity

Fig 2

EFFECTS OF COMPOSITION AND ENVIRONMENT ON THE FRACTURE OF FLUORIDE GLASSES

Stephen W. Freiman and Theresa L. Baker
Ceramics Division
National Bureau of Standards
Gaithersburg, MD 20899

ABSTRACT

Indentation-crack-length procedures were used to determine the critical fracture toughness and the sensitivity to environmentally enhanced crack growth in heavy metal fluoride glasses of varying chemical composition. The data show that while K_{IC} is more or less invariant with composition, some glasses were more susceptible to subcritical crack growth than others. The results are interpreted in terms of existing crack growth models. A technique for predicting K_{IC} from fundamental atomic bonding and crystal structure data for these glasses is discussed.

INTRODUCTION

In recent years there has been considerable interest shown in glasses based on heavy metal fluorides (e.g. ZrF_4 and HfF_4), because of their infrared transmitting properties out to ≈ 7 microns. Heavy metal fluoride glasses are being considered for applications in fiber optic communication lines, infrared transmitting windows, and bulk optical components. In designing any of these components one of the considerations must be the mechanical and thermal loads imposed during service. As will be shown in this paper, these glasses are relatively weak in comparison to normal soda-lime-silica compositions. It will also be shown that their resistance to fracture decreases in the presence of certain chemical environments, including water.

EXPERIMENTAL PROCEDURE

Materials

The fluoride glass compositions investigated in this study are all based on variations in concentrations of ZrF_4 and BaF_2 (Table 1). They were prepared by standard techniques and obtained as plates.[1]

Indentation Technique

The indentation-crack length technique as described by Anstis et al (1) was employed in this study. This technique involves using a Vickers diamond indentation to produce cracks in the polished surface of a glass or ceramic, whose lengths can be measured in an optical microscope. The indentation load (5 N) was chosen to produce well defined radial cracks while minimizing lateral cracking. Measurements were made in different liquids by indenting the specimen through the liquid, then covering the indentation site with a glass cover slide before making the crack length determinations. Five separate indentation crack growth curves were obtained for each glass in water and oil. The critical fracture toughness, K_{IC}, measurements were made in a silicone based diffusion pump oil which had been dried for 16 hours in air at 125°C and stored in a dessicator. Comparisons between environments were made by measuring crack lengths at the same elapsed time after indentation. Because of the time required to transfer the specimen between indenter and microscope, an interval of 30 to 45 seconds between the end of the indentation process and the beginning of the measurement process was maintained.

Critical stress intensity factors, K_{IC}, were calculated from Equation 1 (1):

$$K_{IC} = \phi(E/H)^{\frac{1}{2}} P/c^{\frac{3}{2}}, \qquad (1)$$

---

[1] La Verre Fluore'

where E is Young's modulus (taken to be 56 GPa for all of these glasses (2)), H is the measured hardness (2.4 GPa for all glasses), P is the indentation load (5 N), c_o is the measured crack length in the dry silicone oil, and J is an empirical constant.

RESULTS

The results of the critical fracture toughness determinations on this series of fluoride glasses are presented in Table 1. The values of K_{IC} were calculated using a value for the constant, J, of 0.0109. This value of J was chosen instead of the reported value of 0.016 (1), by normalizing the fracture toughness of soda-lime-silica glass to 0.75 $MPam^{\frac{1}{2}}$, which is the K_{IC} obtained by conventional fracture mechanics techniques. The use of the smaller value of J assumes that glasses show a different indentation behavior than single crystals or polycrystalline ceramics as was noted by Anstis et al (1). The values of K_{IC} given in Table 1 agree quite well with the largest K_I values observed in crack velocity studies (3), and represent a point on the very steep portion of these V-K_I curves. These K_{IC} data strongly suggest that minor variation in glass composition have no effect on fracture toughness. Note that these values of K_{IC} are about one-third of those observed for oxide glasses ($\simeq$0.75 $MPam^{\frac{1}{2}}$).

Crack growth data was taken in four different liquids, dry oil, water, acetonitrile, and heptane. Save for heptane, the indentation crack lengths were measured as a function of time up to 15 minutes. Post-indentation crack growth data for Glasses 2 and 6 are shown in Figures 1a-d as crack length normalized by that taken at zero time (45 sec after indentation) plotted as a function of post-indentation time. These two glasses represent those exhibiting the maximum and minimum crack extension respectively in water compared to oil. Note that for both glasses, the extent of crack extension

with time after the initial 45 sec. delay is significantly greater in oil than in water despite the greater total crack lengths in water. Although in theory (4), values of a crack growth exponent, N, could be calculated from such data, the scatter in the data is too great to place any significance on such values. Nevertheless, it is clear that the extent of crack growth during the 15 minute observation period is greater in the dry oil than in either water or acetonitrile. On the other hand, the actual crack lengths in both water and acetonitrile are significantly greater than in the oil at both the starting time and after 15 minutes, as demonstrated in the plot of crack length, C, normalized by the length, C_{oil}, measured in oil after the same observation period (Figure 2). The increased crack lengths in water and acetonitrile is interpreted as being due to crack growth enhancement in these liquids. The fact that greater crack growth enhancement was measured in acetonitrile than in heptane suggests that it is the acetonitrile molecule rather than water dissolved in the liquid which is producing these results. Heptane is an inert liquid containing approximately 50 ppm. dissolved water. Since the crack lengths in heptane were shorter than those in acetonitrile, it can be concluded that the effects of the dissolved water is less than that of the acetonitrile itself. However, this interpretation is at variance with the V-K_I data reported by Gonzalez (3), which suggests that crack growth in acetonitrile is controlled by the partial pressure of water in the bulk liquid.

The second important observation is that, unlike K_{Ic}, the extent of crack growth in each environment is quite dependent on glass composition. Glass 2 consistently shows the largest ratio of C/C_o, while Glasses 6 and 8 show the smallest (Figure 2).

DISCUSSION

One of the fundamental questions regarding heavy metal fluoride glasses is whether they can be made more fracture resistant through variations in composition or whether the fracture toughness values reported in Table 1 are intrinsic to this class of materials. One way of answering this question is to calculate the intrinsic crack growth resistance of such materials based upon atomic bonding considerations. White et al (5) and Becher and Freiman (6) have shown that an expression derived by Gilman (7) can be used to calculate the fracture energy of a wide variety of single crystals. Agreement between calculated values of ∂ (or K_{IC}) and those measured by conventional fracture mechanics techniques has been excellent (5,6). The following expression can be used to calculate K_{IC}:

$$K_{IC} = \sqrt{2}\ E\ \delta_c/\pi\ d^{\frac{1}{2}} \qquad (2)$$

where E is the Young's modulus of the crystal perpendicular to the crack plane, δ_c is the atomic separation distance at which bond rupture is assumed to take place, and d is the separation distance between cleavage planes.

A basic assumption in making this calculation for these glasses using Equation 2 is that the lack of an ordered crystal structure does not significantly affect the surface energy created by bond rupture. As the simplest example, we assumed that the glass is held together by an array of Zr-F bonds, with other atoms such as Ba, not contributing to the structural network. In making this calculation, we took E to be 56 GPa, the average modulus of the glass (2). δ_c was taken to be the average of the atomic radii of Zr and F, 0.108 nm.(5,7), and d was taken as 0.215 nm., the spacing between the Zr and F atoms in the glass. Inserting these values into Equation 2

yields a value of K_{IC} of 0.19 $MPam^{\frac{1}{2}}$, in reasonable agreement with the measured values given in Table 1.

We can improve the calculations somewhat by taking into account the fact that some of the structural bonding in these glasses is contributed by the Ba-F bonds as well the Zr-F bonds. In this case we took δ_c = 0.125 nm., the average of the Zr-F and Ba-F atomic radii, weighted according to their atomic fraction in the glass, and d to be the weighted average of the Zr-F and Ba-F distances (0.233 nm.), yielding a value of K_{IC} of 0.21 $MPam^{\frac{1}{2}}$. The small difference between calculated and measured values of K_{IC} could be due to the random orientation of bond angles with respect to the plane of fractue, which would tend to reduce the stress paralled to each bond. These calculations strongly suggest that the low toughness of these glasses is intrinsic to the material, so that any strengthening must be brought about by other than simple compositional variations.

The environmentally enhanced crack growth behavior in these glasses is more difficult to understand. For instance, no obvious explanation for the distinct composition dependence to crack growth seen in Figure 2 can be put forth. The variations in composition in these glasses is relatively small (Table 1) and show no systematic trend. It is also difficult to classify their crack growth behavior in terms of the atomic bonding. These glasses are ionic materials and so would be expected to show the same behavior as that reported by Michalske et al (8) for magnesium fluoride, namely a strong crack growth enhancement in acetonitrile. The indentation data reported herein suggests that acetonitrile is effective in causing crack growth, but the crack growth data of Gonzalez (3) indicates that it is not. This difference can not be re ved at the present time. The extreme dissolution rate of these glasses in water also appears to complicate the crack growth process.

Dissolution in water leading to changes in crack tip geometry may account for the greater crack extension with time in oil compared to that in water, shown in Figure 1. That is, even the small partial pressure of the water in the oil is sufficient to cause the cracks to grow. In water, competing effects of water on dissolution and crack growth lead to a much smaller crack extension. Another possibility which should not be overlooked is effects of the complex shape of the V-K_I curves for oil and water (3). Since the K_I, and hence crack velocity, is a decreasing function of crack size for the indentation induced cracks, the V-K_I, path which is followed for each environment will play a role in determining the measured crack length.

CONCLUSIONS

Indentation-crack length data was taken for a series of heavy metal fluoride glasses in four liquid environments. Based upon this data it was concluded that the critical fracture toughness of these glasses was low, ≈ 0.25 MPam$^{\frac{1}{2}}$, and independent of glass composition, while their susceptibility to environmentally enhanced crack growth was compositionally dependent. Predictions of K_{IC} based upon atomic bonding condiderations agreed reasonably well with measured values, and implied that the low toughness of these glasses is an intrinsic property of the material. Small quantities of water dissolved in a nominally dry oil were shown to be sufficient to cause crack growth.

ACKNOWLEDGEMENTS

The authors gratefully acknowledge the financial support of this work by the Office of Naval Research. We also thank Bernie Bendow and Jack Mecholsky for supplying the glasses. The numerous helpful discussions with Armando Gonzalez and Grady White are gratefully appreciated.

REFERENCES

1. G.R. Anstis, P. Chantikul, B.R. Lawn, and D.B. Marshall, "A Critical Evaluation of Indentation Techniques for Measuring Fracture Toughness: I, Direct Crack Measurements," J. Am. Ceram. Soc., 64, [9], 533-38, (1981).

2. B. Bendow, E. Hartouni, and J.J. Mecholsky, "Progress in the Fabrication of Mid-Infrared Optical Fibers," SPIE, Int. Soc. for Optical Fibers, 357, (1982).

3. A.C. Gonzalez, "Slow Crack Growth in Fluorozirconate Glass," Master of Science Thesis, Pennsylvania State University, (1987).

4. P.K. Gupta and N.J. Jubb, "Post-Indentation Slow Growth of Radial Cracks in Glasses," Comm. Am. Ceram. Soc., 63, [8], C112-114, (1981).

5. G.S. White, S.W. Freiman, E.R. Fuller, Jr., and T.L. Baker, "Effects of Crystal Bonding on Brittle Fracture" submitted for publication to J. Mater. Res.

6. P.F. Becher and S.W. Freiman, "Crack Propagation in Alkaline-Earth Fluorides," J. Appl. Phys., 49, [7], 3779-83, (1978).

7. J.J. Gilman, "Direct Measurements of the Surface Energies of Crystals," J. Appl. Phys., 31, [12], 2208-18, (1960).

8. T.A. Michalske, B.C. Bunker, and S.W. Freiman, "Stress Corrosion of Ionic and Mixed Ionic/Covalent Solids," J. Am. Ceram. Soc. 69, [10], 721-24, (1986).

FIGURE CAPTIONS

Figure 1. Normalized indentation crack lengths as a function of time for Glasses 2 and 6 tested in water and oil. C_o is the crack length at the start of measuring, about 45 seconds after indentation. Where less than five data points are shown, some of the individual measurements were indistinguishable.

Figure 2. Indentation crack lengths measured after 5 minutes (open symbols) and 15 minutes (closed symbols) for all glasses tested in various environments. The measured crack length in a particular environment was normalized by that taken in oil after the same waiting period.

TABLE 1

Heavy Metal Fluoride Glass Compositions and Critical Fracture Toughness

COMP#	ZrF_4	BaF_2	LaF_3	AlF_3	HoF_3	ThF_4	GdF_3	K_{IC}
2	60.5	33.5	3.5	2.5	--	--		.25
3	57	35	5	3	--	--		.23
4	55.5	33	5	5.5	--	--		.22
5	58.1	34.2		3.6	--	--	4.1	.25
6	59	32.8	--	3.6	--	4.6		.23
8	58	34.5	--	4.5	3	--		.22

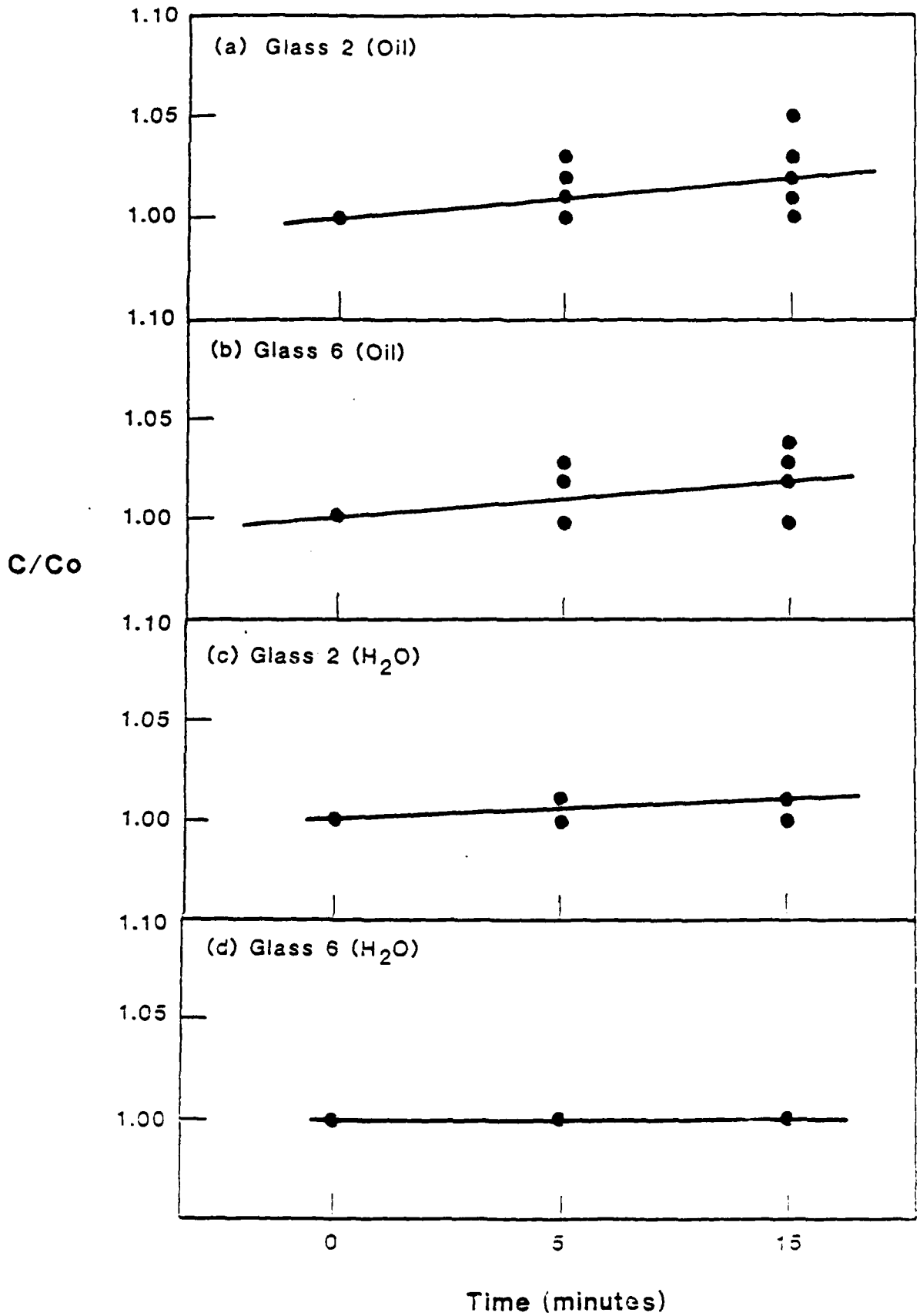
(a) Glass 2 (Oil)
(b) Glass 6 (Oil)
(c) Glass 2 (H_2O)
(d) Glass 6 (H_2O)
1.10
1.05
1.00
C/Co
0
5
15
Time (minutes)

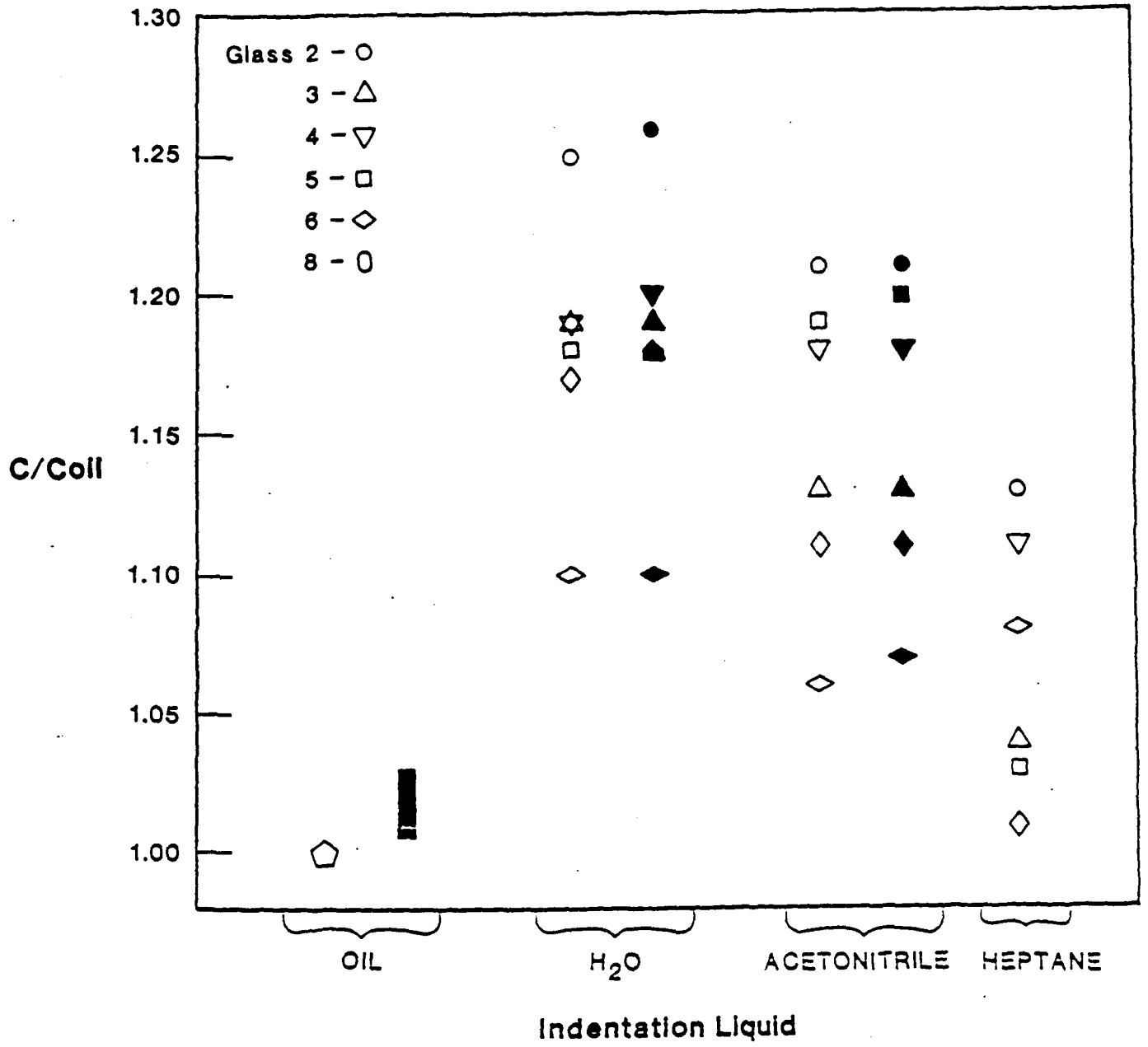
1.30
1.25
1.20
1.15
1.10
1.05
1.00
C/Coil
Glass 2 - ○
3 - △
4 - ▽
5 - □
6 - ◇
8 - ⬠
OIL
H2O
ACETONITRILE
HEPTANE
Indentation Liquid

YOUNG'S MODULUS AND THERMAL DIFFUSIVITY MEASUREMENTS OF BARIUM TITANATE BASED DIELECTRIC CERAMICS

G. S. White and C. Nguyen
National Bureau of Standards
Gaithersburg, MD 20899

Bharat Rawal
AVX Corporation
Myrtle Beach, SC 29577

ABSTRACT

Young's modulus and thermal diffusivity values have been obtained on a set of barium titanate based ceramics using ultrasonic pulse-echo and photoacoustic effect (PAE) measurements. The PAE was shown to detect variations in thermal diffusivity between materials of varying composition and processing treatments. The results are valuable in the evaluation of dielectric ceramic materials for practical electronics applications.

INTRODUCTION

The use of multilayer ceramic capacitors (MLCs) is rapidly increasing in surface mount applications and, therefore, the understanding of mechanical properties and thermal shock resistance parameters of these materials is becoming increasingly important. Of the various soldering techniques utilized in surface mount applications, including wave soldering, vapor phase soldering and infrared reflow techniques, wave soldering imposes the most severe thermal stresses on the materials[1,2] since it involves rapid surface heat transfer from the molten metal to the terminations of the MLCs. The rapid heat transfer in processes like wave soldering results in large temperature gradients and the resulting stresses in the capacitors are further complicated by differences in the coefficients of thermal expansion and thermal diffusivities between the capacitors and other materials used in the surface mount manufacturing processes. Temperature gradients may lead to crack initiation and/or crack propagation which in turn may contribute to the subsequent deterioration of the insulation resistance of capacitors. Because barium titanate materials are often used as the major componants of MLCs, there is considerable interest in the determination of the initial flaw sources and distribution, in the elastic and thermal properties, and in mechanisms by which these flaws initiate and propagate in barium titanate based dielectric materials. This work reports the results of nondestructive evaluation (NDE) measurement techniques of

the Young's modulus and thermal diffusivity of several $BaTiO_3$ based dielectric ceramics.

EXPERIMENTAL PROCEDURE

Specimens were prepared by using standard capacitor manufacturing techniques[3] using the tape cast process with various dielectric compositions classified by the Electronic Industry Association (EIA) temperature characteristics referred to as X7R and Z5U ceramics. Specimens with dimensions of 25 x 25 x 3.0 mm were designated as X7R-1, X7R-2, Z5U-1, Z5U-3, and Z5U-3nb where X7R-1 and 2 are barium-bismuth titanate based dielectrics containing different minor constituents, Z5U-1 is a barium titanate-calcium zirconate based ceramic, and Z5U-3 and Z5U-3nb are relaxor based ceramic materials which are similar in composition but are processed differently.

Young's moduli for the specimens were obtained using standard ultrasonic pulse-echo measurements. Measurements were made at 10 MHz, and, for both longitudinal and shear wave velocities, data were taken for 1, 2, and 3 transit times of the specimen. Uncertainty in the velocity measurements was $\leq 1.5\%$ and in the specimen density was $\leq 1\%$. Therefore, the uncertainty in E was $\leq 2.5\%$.

Values for the thermal diffusivities were obtained using the photoacoustic effect (PAE) technique following Pessoa et al.[4]. All specimens first were ground on both sides by a 600 grit diamond wheel to a final thickness of 0.59 mm. For purposes of comparison, the thermal diffusivity of an alumina specimen (0.64 mm thick) was also measured. Photoacoustic measurements were made using the apparatus shown in Fig. 1.

Specimens were mounted in an aluminum PAE cell with a thin layer of vacuum grease as the bonding medium. Modulated radiation from a CO_2 laser, operated at 600 mW, was directed either to the front of the specimen (inside the chamber) through a ZnSe window or to the rear of the specimen through a 6x8 mm rectangular hole in the rear of the chamber. Laser beam modulation was achieved through the use of a mechanical chopper and frequencies ranged from 0.87 Hz to 100 Hz. The PAE signal detected by the microphone was filtered by a vector lock-in amplifier, from which phase measurements of the signals resulting from front and rear surface heating were obtained. The frequency was monitored by an independent meter.

The PAE parameter of interest was the phase difference between front surface and rear surface heating obtained as a function of heating frequency. For some maximum frequency, f_M, the phase difference would become independent of frequency. At higher frequencies, $f>f_M$, the modulated thermal signal was unable to penetrate the specimen. Because f_M depended on the thermal properties of the particular specimen, it was not possible to predict its value precisely. Therefore, the upper limit of 100 Hz was arbitrarily chosen since it was expected that $100\ Hz \gg f_M$. The lower frequency limit, 0.87 Hz, was at the limit of the frequency response of the apparatus.

RESULTS AND DISCUSSION

Young's Modulus

Table I shows the values for the Young's moduli obtained for the five specimens:

Table I:

Specimen	Density g/cc	Young's Modulus GPa	Thermal Diffusivity ($\times 10^{-3}$ cm^2/s)
X7R-1	5.875	148.0	5.63
X7R-2	5.834	105.0	12.35
Z5U-1	5.669	143.2	8.92
Z5U-3	8.095	131.2	4.88
Z5U-3nb	7.650	112.1	4.95

These values vary from 105.1 GPa for the X7R-2 specimen to 148.0 GPa for the X7R-1 specimen. While part of this change can be explained by changes in the compositions of the specimens, e.g. the change from 148 GPa for X7R-1 to 112.1 GPa for Z5U-3nb, some of the variation in Young's modulus must result from processing conditions, as shown by the fact that, although the Z5U-3 and the Z5U-3nb specimens are compositionally the same, E changes from 131.2 GPa for the former to 112.1 GPa for the latter. The change in the E values for the Z5U-3 and Z5U-3nb specimens reflects the fact that E is a function of the density, ρ, as well as of the longitudinal and shear wave velocities of the materials. All three of these physical parameters can vary for different processing conditions.

Because the Young's modulus is the measure of the change in stress in a material resulting from a given change in strain, it is reasonable to expect that the probability of mechanical failure resulting from thermal shock would increase with increasing E. This is certainly true for some geometries, in which the thermal stresses are proportional to E^5.

Thermal Diffusivity

The thermal diffusivities (α) of the specimens, as determined using front and back heating in the PAE, have also been obtained and are shown in Table I. α is related to the difference in the phases of the PAE signal for front and rear surface heating, $\Delta\phi$, by the following expressions 4:

$$\alpha = \omega/(2a^2) = k/(\rho C)$$

$$\tan(\Delta\phi) \approx \tanh(al)\tan(al) \qquad (1)$$

where ω is the angular modulation frequency of the heating beam, l is the specimen thickness, a is defined by eqn. 1 and is the inverse of the thermal diffusion length, k is the thermal conductivity, and C is the heat

capacity of the specimens. To evaluate α, the experimentally obtained values of $\Delta\phi$ and the calculated values, $\tan^{-1}(\tanh(la)\tan(la))$, were plotted as functions of la. Because $la = l(\omega/(2\alpha))^{1/2}$, estimates of α were adjusted to obtain the best agreement between the measured and calculated values of $\Delta\phi$. Figure 2a is a plot of $\Delta\phi$ vs la for the alumina specimen, which was used to evaluate the accuracy of the technique for the determination of α. The symbols in the figure represent the experimental values and the solid line is calculated from eqn. 1 resulting in a value $\alpha = 0.087$ cm^2/s. This value of α is in agreement with the literature values[6] of α calculated from the thermal conductivity, K, specific heat, C, and density, ρ. To show the sensitivity of eqn. 1 to α, Figure 2b is a plot of the same experimental data but, this time, the solid line corresponds to $\alpha = 0.096$ cm^2/s, a change of 10% from the previous value. The curve in Fig. 2a fits the data better than the curve in Fig. 2b, showing that eqn. 1 can determine values of α within at least 10%.

Both Figs. 2a and 2b show a deviation of the data from the calculated line for higher values of la (i.e. for modulation frequencies > f_M). As mentioned previously, this deviation derives from the thermal thickness of the specimen being greater than the propagation distance of the modulated heat flow, at least within the sensitivity of the experimental apparatus.

Specifically, for an alumina specimen 0.64 mm thick, with $\alpha = 0.087$ cm^2/s, the measured values of $\Delta\phi$ deviate from the calculated values and, in fact, become constant, for $la \geq 2.8$. It must be borne in mind, however, that the value of la at which $\Delta\phi$ levels off results only from a limit in the sensitivity of the experimental apparatus, not from a change in the physical processes giving rise to the signal and, in addition, this value of la is not dependent upon the thermal properties of the specimens.

Because the upper limit of la for which measurements can be made depends only on the sensitivity of the detection apparatus, it should be the same for all materials. This is shown in Fig. 3(a-d) which gives both experimental and calculated values of $\Delta\phi$ for X7R-1, X7R-2, Z5U-1 and Z5U-3. In all cases, the calculated values deviate from the experimentally obtained values at $la \approx 2.8$. This result implies that a second method of determining α is to plot $\Delta\phi$ vs f, where f is the heating modulation frequency (Fig. 4). At the frequency, f_M, at which $\Delta\phi$ becomes independent of f,

$$\alpha \approx (1/2.8)^2(f_M\pi). \qquad (2)$$

The value 2.8 is an experimental parameter, of course, and must be determined for each PAE system. Table II lists the values and uncertainties of α determined by the two methods:

Table II: Thermal Diffusivity ($x10^{-3}$ cm^2/s)

Specimen	α_{eqn1}	±	α_{eqn2}	±
X7R-1	5.63	0.65	7.0	1.1
X7R-2	12.35	1.22	15.5	2.5
Z5U-1	8.92	1.93	9.1	4.9
Z5U-3	4.88	0.55	8.4	0
Z5U-3nb	4.95	0.73	6.7	2.5

The results shown in the Table indicate that α varies by more than a factor of two among the different materials. In particular, the thermal diffusivities of X7R-1 and X7R-2 change from 5.63 cm^2/s to 12.35 cm^2/s and a similar change occurs for Z5U-1 and Z5U-3. Interestingly, there is no meaningful change in α between Z5U-3 and Z5U-3nb, as determined by fitting the data to the expression in eqn. 1. Another feature shown by Table II is that the uncertainties which result from calculating α using the deviation of $\Delta\phi$ from a constant value are much larger than those obtained using eqn. 1. The increase in the uncertainty of α results from the finite number and spacing of the experimental values of the frequency. This problem is aggravated by the low thermal diffusivities of the materials under investigation. Even though the specimens were machined to ≈600 μm in thickness, the frequencies which would allow the thermal waves to penetrate the specimen were below 15 Hz. Since α, determined by the deviation of $\Delta\phi$ from a constant value, is directly proportional to the frequency at which the deviation occurs (eqn. 2), even a 1 Hz change in determining f_M would correspond to a 7% change in α. For the X7R-1, Z5U-3, and Z5U-3nb specimens, the upper frequency limit was even lower, resulting in larger changes in α for a 1 Hz change in f_M. In comparison, eqn. 1 allows much finer determinations of α because an entire range of data points is being used to fit the calculated curve. Therefore, although the data are restricted to the same frequency range, a change in the value of the phase measured at f_M will have much less effect on the determination of α. Therefore, while evaluating α by eqn. 2 is straight forward and provides reasonable approximations of α, fitting the data to eqn. 1 results in more accurate values of α with less uncertainty.

Behavior of these materials under thermal stress

For rectangular geometries, it has been shown[5] that the thermal stresses in the materials will increase with increasing values of E and with decreasing values of α. Figure 5 is a plot of E/α for the five materials. The larger the E/α ratio, the more susceptible the material should be to thermal shock, provided that other parameters like coefficient of thermal expansion are similar. A study of the thermal susceptibility of capacitor chips manufactured[2] from these materials in fact demonstrates that X7R-1 is more susceptible to thermal shock compared to X7R-2; however, similar results were not obtained when Z5U-1 and Z5U-3 were compared because the coefficients of thermal expansion were significantly different.

CONCLUSIONS

Thermal and ultrasonic waves have been used to measure thermal diffusivities and Young's moduli in a set of barium titanate based and relaxor dielectric materials and these measurements have been used to clarify the behavior of these materials under thermal stress applications.

ACKNOWLEDGEMENTS

We would like to thank the Office of Nondestructive Evaluation at the NBS, the Office of Naval Research, and the AVX Corporation for their support of this work. We also thank E. Krasicka for assistance in setting up the ultrasound experiments.

REFERENCES

1. J. Maxwell, "Surface Mount Soldering Techniques and Thermal Shock in Multilayer Ceramic Capacitors," AVX Technical Information Series (1987) 4pp.
2. B. Rawal, R. Ladew, and R. Garcia, "Factors Responsible for Thermal Shock Behavior of Chip Capacitors," Proc. of the 37th Electronic Components Conference, Boston, MA (1987) pp.145-156.
3. M. Kahn, "Multilayer Ceramic Capacitors - Materials and Manufacture," AVX Technical Information Series (1981) 5pp.
4. O. Pessoa, Jr., C. L. Cesar, N. A. Patel, H. Vargas, C. C. Ghizoni and L. C. M. Miranda, "Two Beam Photoacoustic Phase Measurement of the Thermal Diffusivity of Solids," J. Appl. Phys. 59 (4), (15 Feb. 1986) pp.1316-1318.
5. W. D. Kingery, H. K. Bowers and D. R. Uhlmann, Introduction to Ceramics, 2nd Edition, John Wiley and Sons, New York (1976) p.820.
6. Coors Alumina and Beryllia Properties Handbook, Bulletin 952, Coors Porcelain Company, Golden, CO (1969) pp.6-7.

FIGURE CAPTIONS

Figure 1: Schematic of photoacoustic apparatus. A mirror could be inserted or retracted to direct the modulated heating beam through the ZnSe window at the front or through a hole blocked by the specimen at the rear of the photoacoustic cell.

Figure 2: Plots of calculated and measured values of $\Delta\phi$ vs la for a dense Al_2O_3 specimen. a) Solid line calculated assuming $\alpha=.087$ cm^2/s. b) Solid line calculated assuming $\alpha=.094$ cm^2/s. Deviation of calculated values from measured values of $\Delta\phi$ begins at $la\approx 2.8$.

Figure 3: Calculated and measured values of $\Delta\phi$ plotted vs la for a) X7R-1, b) X7R-2, c) Z5U-1, and d) Z5U-3 specimens. Figure shows that data for all specimens begin deviating from calculated values at $la\approx 2.8$. At lower values of la, there is agreements between experimental and calculated values of $\Delta\phi$.

Figure 4: $\Delta\phi$ vs frequency for Z5U-1 specimen showing that $\Delta\phi$ levels off to essentially a constant value for $f\geq 9$ Hz.

Figure 5: Values of thermal diffusivity for the 5 specimens which were investigated. The figure shows the range of values obtained in separate series of experiments.

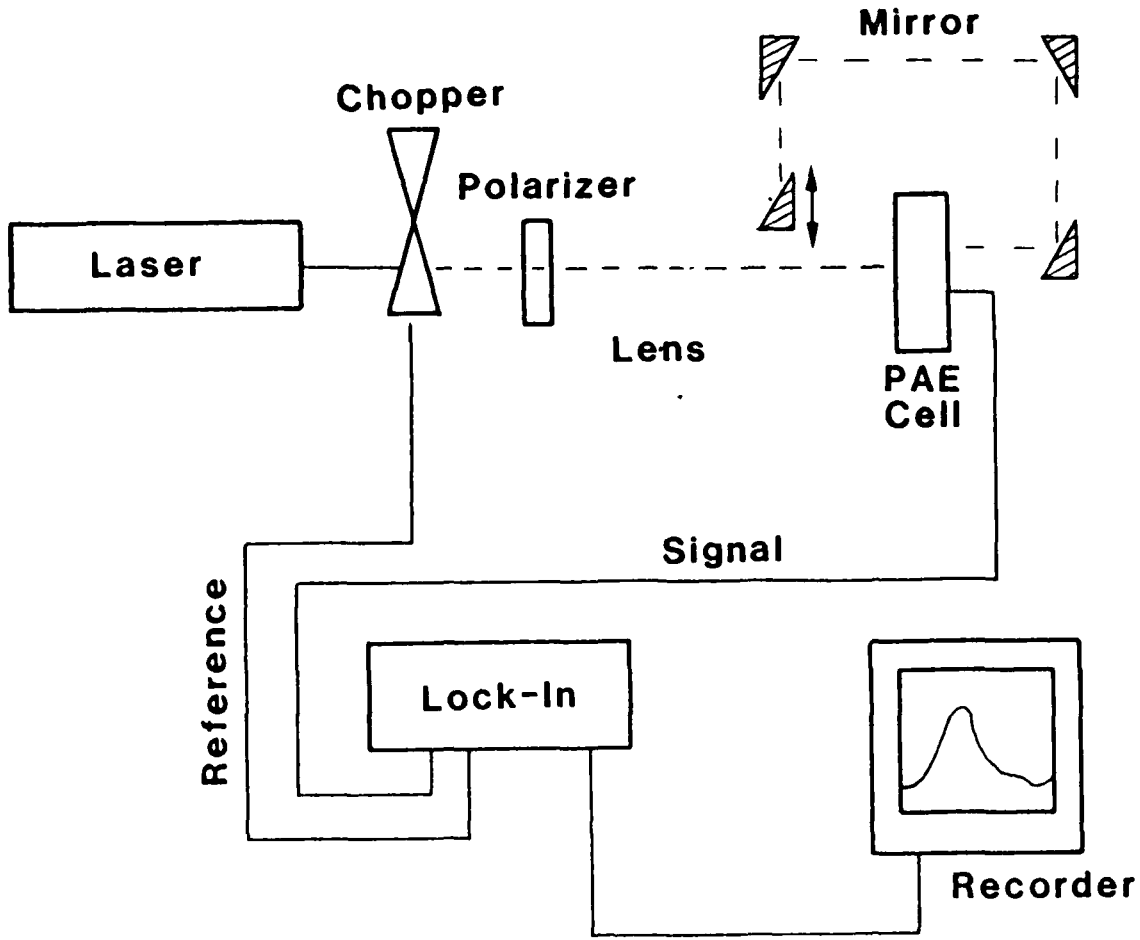
Mirror
Chopper
Polarizer
Laser
Lens
PAE
Cell
Signal
Reference
Lock-In
Recorder

Fig 1

Fig 2

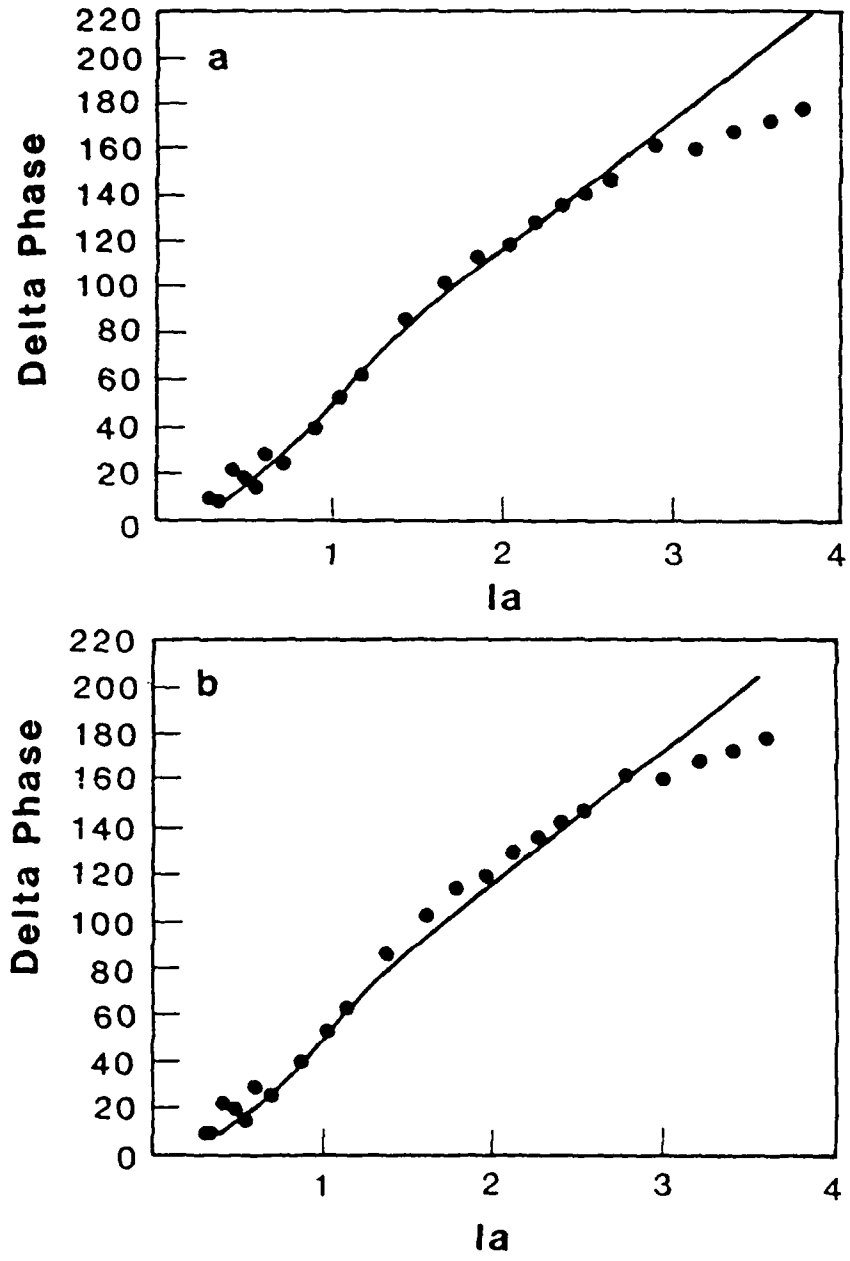
a
Delta Phase
220
200
180
160
140
120
100
80
60
40
20
0
1
2
3
4
Ia
b
Delta Phase
220
200
180
160
140
120
100
80
60
40
20
0
1
2
3
4
Ia

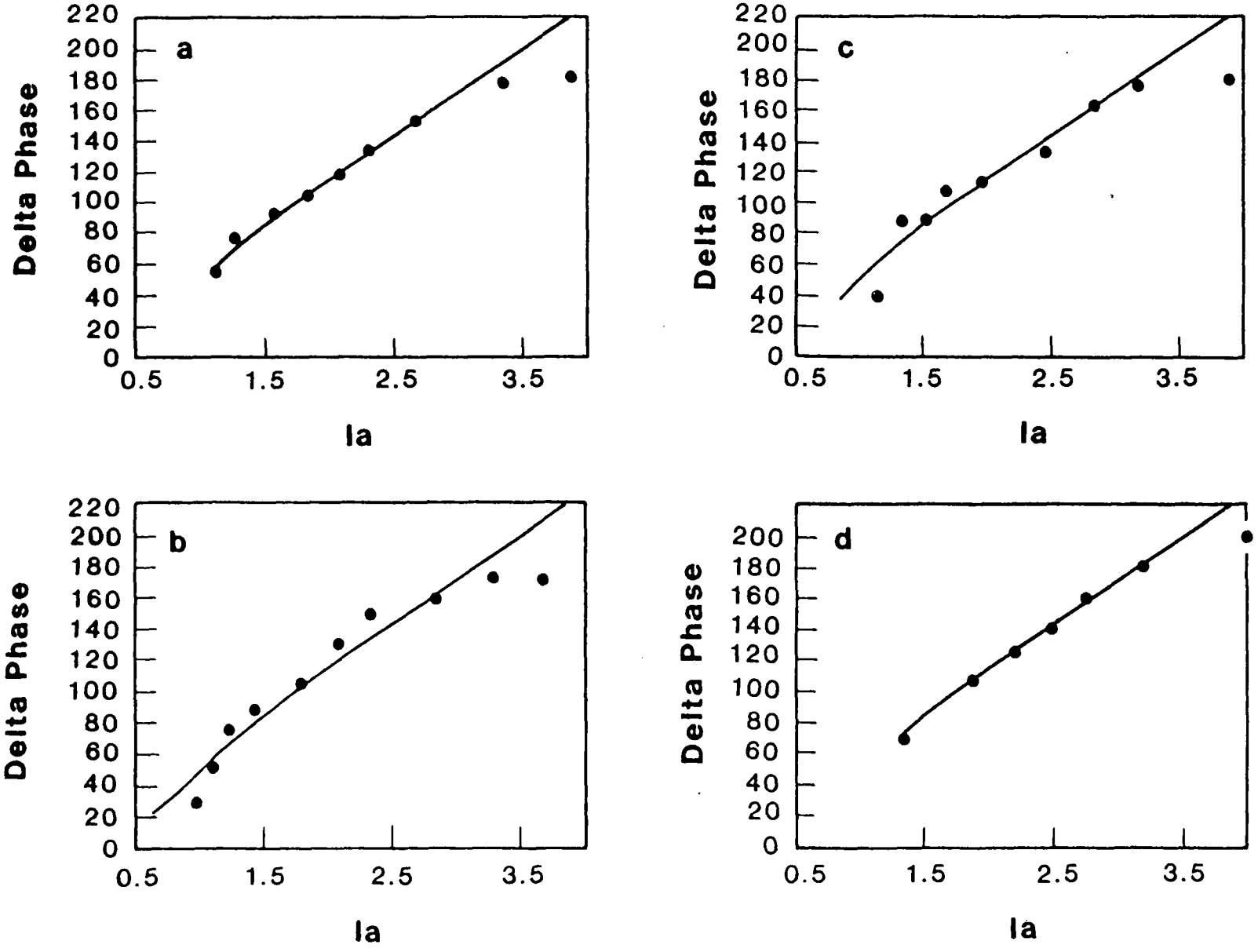
a
b
c
d
Delta Phase
Ia
0
20
40
60
80
100
120
140
160
180
200
220
0.5
1.5
2.5
3.5

Fig 3

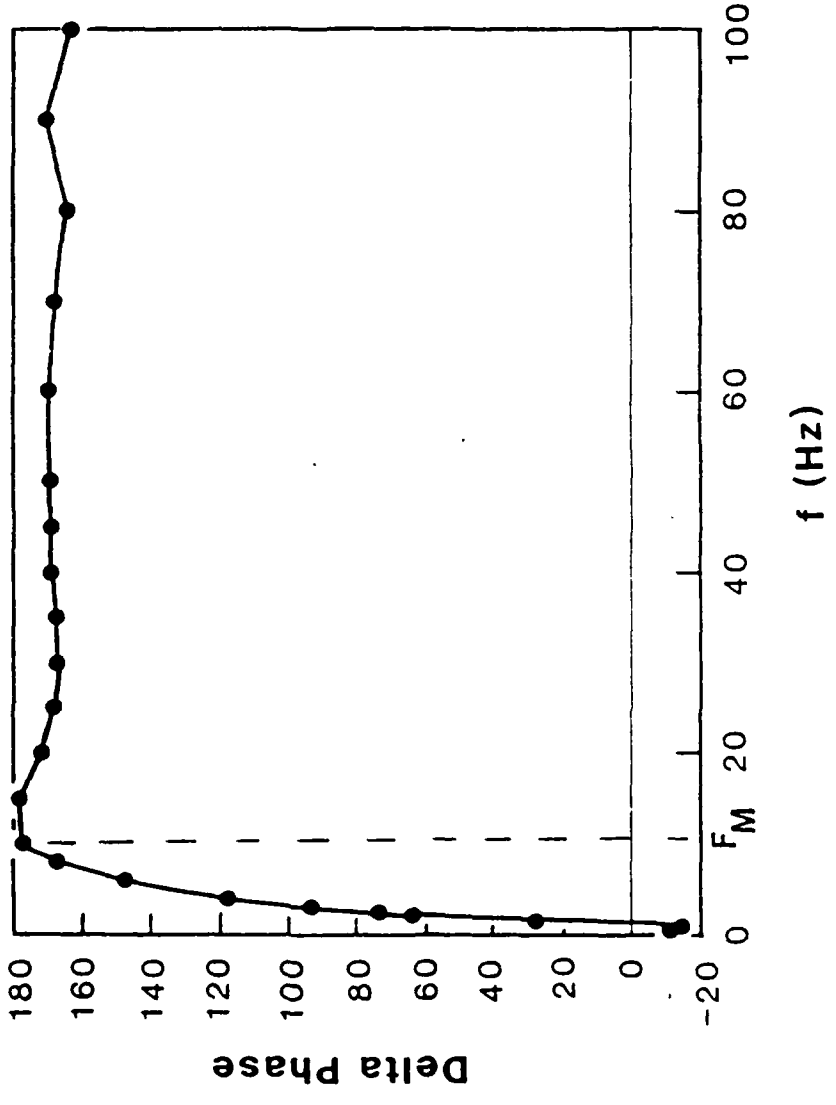
Delta Phase
180
160
140
120
100
80
60
40
20
0
-20
0
F_M
20
40
60
80
100
f (Hz)

Fig 4

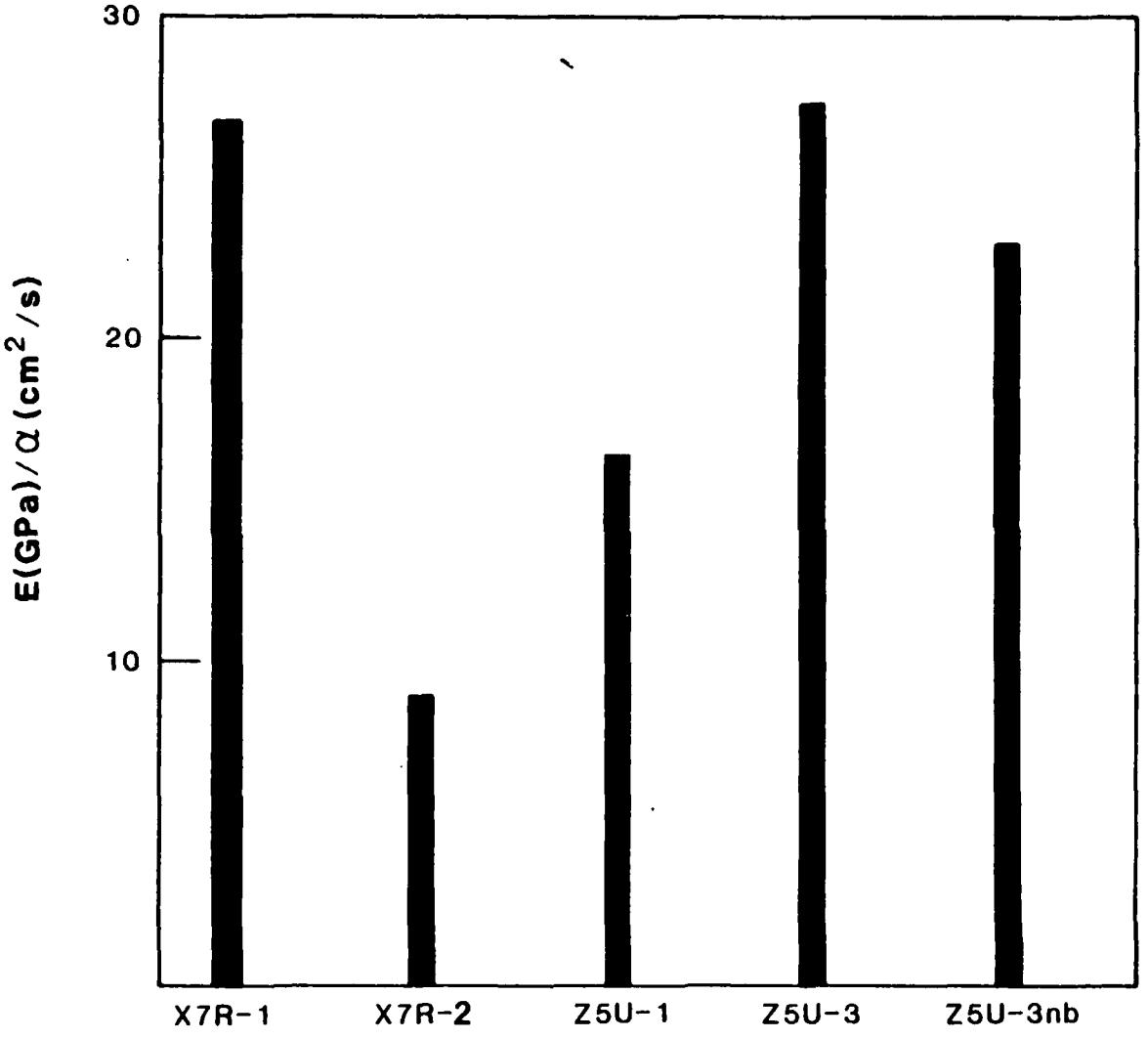
30
20
10
E(GPa)/α (cm²/s)
X7R-1
X7R-2
Z5U-1
Z5U-3
Z5U-3nb

Fracture Behavior of Electronic Ceramics

Stephen W. Freiman
Ceramics Division
National Bureau of Standards,
Gaithersburg, MD

Abstract

This paper reviews the fracture behavior, including the strength, fracture toughness and susceptibility to environmentally enhanced crack growth of dielectric and piezoelectric ceramics such as barium titanate and lead zirconate titanate (PZT). Polycrystalline ceramics are known to exhibit a critical fracture toughness, K_{IC}, as measured by classical fracture mechanics techniques, which depends strongly on grain size, and in the case of PZT, chemical composition and phase content. It is shown that fracture toughness models can be used to predict microstructures which improve crack growth resistance. The micro-structure of these ceramics has a direct effect on the strength of an electrical component as well as influence its resistance to the growth of large cracks. For instance, the paraelectric to ferroelectric phase transformation in barium titanate, PZT, and related ceramics induces internal stresses which provide an additional driving force for flaw extension. Finally, crack growth rates in electronic ceramics are accelerated by the presence of moisture in the environment. Such environmentally enhanced crack growth can have a significant effect on failures of electrical components since flaws will grow with time under a relatively low static stress.

DURING THE PAST FEW YEARS, as new devices and applications involving electronic ceramics have been developed, interest and concern over the mechanical reliability of these materials has increased. These applications can involve the dielectric as well as the piezoelectric or ferroelectric properties of the material. In this paper we bring together a number of the concepts discussed in the literature over the past few years, and show that

the fracture behavior of these sometimes quite different materials can be understood through the application of a few general models. This paper is divided into sections, each discussing the critical aspects of the mechanical behavior of a particular set of materials, followed by a summary which presents an overall picture of their fracture properties.

BARIUM TITANATE

Barium titanate is used in two classes of materials, one which makes use of its piezoelectric/ferroelectric properties (e.g., transducers) and one which employs the large dielectric constants attainable in modifications of this ceramic (e.g., multilayer capacitors).

PIEZOELECTRIC BARIUM TITANATE - One of the most important observations regarding the fracture behavior of ferroelectric materials was made by Pohanka et al (1) in 1976. These authors found that strengths of polycrystalline barium titanate measured above the Curie temperature were ≈ 50% greater than those measured at room temperature, and that this difference was essentially independent of grain size (Figure 1). Based upon this strength difference, Pohanka et al concluded that internal stresses generated during the cubic to tetragonal phase transformation added to the applied stress to lower the strength of the material at room temperature. The values of internal stress calculated from the strength difference were shown to be in good agreement with those predicted by Buessem et al (2) from permittivity measurements.

In a more recent study, Cook et al (3) followed up on this work using an indentation-fracture technique to investigate both the fracture toughness and

internal stress effects in both commercial barium titanate (grain size = 7 microns) and one of the experimental materials prepared by Pohanka et al (1) (grain size = 1 micron). The advantage of the indentation-fracture procedure is that a Vickers hardness indenter can be used to create a flaw of known size and which is driven by a well characterized stress field. The results of this study are demonstrated for the commercial barium titanate in the logarithmic plot of fracture stress versus indentation load shown in Figure 2. The slopes of the curves in the large indentation load regime are -1/3 as predicted from the indentation fracture model (4). The critical fracture toughness of the material can be calculated from the position of these curves using an expression derived by Chantikul et al (4). These calculations yield values of K_{IC} of 1.1 MPam$^{\frac{1}{2}}$ and 1.5 MPam$^{\frac{1}{2}}$ for the cubic and tetragonal material respectively. Cook et al also showed that K_{IC} decreased monotonically with temperature through the Curie point. The increased toughness of barium titanate in the tetragonal state had already been demonstrated by Pohanka et al (5), who showed that the increased K_{IC} could be ascribed to cracks interacting with 90° domains in the structure. These domains exist in tetragonal but not in cubic barium titanate. A similar difference in K_{IC} above and below the Curie point was reported by de With and Parren (6) for modified barium titanate.

The deviation of the strengths at small loads from the indentation model in Figure 2 for the tetragonal material is indicative of the increasing influence of the internal stresses as the flaw size decreases relative to the microstructure. The difference in strength between the tetragonal and cubic material is approximately 56 MPa, essentially that calculated earlier by Pohanka et al (1). Experiments performed on barium titanate made

semiconducting by the additions of a small quantity of samarium indicate that the level of internal stress is not reduced by increasing the conductivity of the material (7), leading to the conclusion that the internal stresses are not due to the formation of space charges in the material.

Figure 2 structural strength of a commercial barium titanate tested above and below the Curie temperature as a function of the indentation load used to introduce the flaw. All failures occurred from the indentation. The straight lines through the data at 25°C and 150°C represent the best fit line of slope, -1/3, following the indentation-fracture model (4). The deviation in the 25°C data from the model is ascribed to the contribution of internal stresses (after Cook et al(3)).

It has also been shown that in the ferroelectric state the fracture energy of polycrystalline barium titanate is a function of grain size, while that for cubic material is independent of grain size (Figure 3) (7). The grain size dependence of fracture energy for the tetragonal material was explained in terms of a combination of 90° domain and microcracking enhanced toughening in the material. The maximum fracture energy occurs at a grain size of 40 microns due to a tradeoff between the generation of microcracks at the primary crack tip, a process which reduces the driving force on the crack, and the linking of the microcracks, which at large grain sizes produces spontaneous failure of the material. It was shown that this complex behavior could be fit to a general model for the fracture energy of non-cubic ceramics derived by Rice and Freiman (8).

Barium titanate, like almost all ceramics, is sensitive to moisture enhanced crack growth. The moisture enhanced fracture process can be characterized by measuring the strength of the material as a function of

stressing rate as shown in Figure 4. The slope of this plot can be used to calculate a value for N the exponent in the crack growth expression:

$$V = Vo(K_I/K_{IC})^N \qquad (1)$$

where V is the crack velocity, K_I is the stress intensity factor at the crack tip, and Vo and N are empirical constants that depend on material and environment. Typical values of N range from 15 to 70, with the lower values associated with more stress corrosion susceptible materials.

CERAMIC CAPACITORS - Multilayer ceramic capacitors are generally composed of barium titanate and related compounds whose mechanical properties can be characterized in the same way as barium titanate. Indentation-fracture techniques have been used to determine the strength, fracture toughness and subcritical crack growth behavior in a number of capacitor ceramics (9). Fracture toughness values range from 0.7 to 1.4 $MPam^{\frac{1}{2}}$ depending on the particular capacitor composition.

Like the previous materials, capacitor ceramics also undergo slow crack growth in the presence of water. Their susceptibility to crack growth in water varies markedly from one capacitor composition to another, probably because of differences in the chemistry of the material.

PZT

Unlike barium titanate, which in general can be thought of as a single compound ($BaTiO_3$), PZT occurs as a series of solid solutions of PbZr03 with

$PbTiO_3$, and can exist in various crystal structures (10). As with barium titanate, the fracture toughness of PZT is significantly higher in the ferroelectric state than in the paraelectric state for all PZT compositions (7,11), with the larger value of K_{IC} in the ferroelectric material again being partially due to crack-twin interactions which cannot occur above the Curie temperature. In PZT, we can also examine the effect of changing chemistry on the fracture behavior of the material in the ferroelectric state. The room temperature fracture toughness of PZT over a range of Zr/Ti ratios is presented in Figure 5. The data appear to pass through a series of maxima and minima in K_{IC}, with a very distinct minimum occurring at the morphotropic boundary between the tetragonal and rhomobohedral phases. The other minima in K_{IC} also appear at phase boundaries. It was concluded by Freiman et al (11) that these minima were due to a trade-off between contributions to K_{IC} of twin crack interactions and microcracking. Because twin motion is easier at phase boundaries, the internal stresses and therefore the degree of microcracking will be minimized at these compositions, leading to minima in fracture toughness. The data in Figure 5 is similar to that obtained by Igarashi and Okazaki (12) who showed that both strength and K_{IC} are a minimum at the morphotropic boundary.

At PZT compositions near 95% $PbZrO_3$ -5% $PbTiO_3$, i.e. near the boundary between the ferroelectric, rhombohedral phase and the antiferroelectric phase, it was observed that if the material is electrically poled and subsequently depoled by the application of hydrostatic pressure, the fracture toughness increases by 50%. Freiman et al (11) hypothesized that the additional toughening brought about by pressure depoling is due to the stress induced transformation of antiferroelectric domains in the vicinity of the crack tip.

These domains exist in what should otherwise be a single ferroelectric phase because the pressure induced transformation from ferroelectric to antiferroelectric phases is not fully reversible (13) so that upon removal of the pressure, remnants of the antiferroelectric phase remain. The presence of residual antiferroelectric domains in the ferroelectric material has been determined both microscopically (14) and electrically (15). Freiman et al (11) also showed through indentation-fracture measurements, that the fracture toughness of 95/5 PZT is sensitive to the lead content in the material (Figure 6). As the stoichiometry of the material was varied toward increasing lead content, K_{IC} decreased from approximately 1.7 to 1.2 $MPam^{\frac{1}{2}}$. The composition having the highest K_{IC} is also the one showing the largest ratio of transgranular to intergranular fracture. Conversely, the lowest toughness material showed almost entirely intergranular fracture, implying that the excess lead contributes to the relative weakness of the grain boundaries. In addition, Freiman et al (11) used the indentation-fracture data in Figure 6 to demonstrate the existence of internal stresses in this material. The magnitude of internal stress, as determined by the deviation of data from the indentation model at small indentation loads, varied with the stoichiometry of the material. The minimum effective internal stress is observed at approximately the lead content corresponding to the stoichiometric compound. This minimum in internal stress occurs at the same composition at which the greatest symmetry in the electrical polarization curves is observed, in agreement with the data of Dungan and Storz (16).

Like barium titanate, PZT undergoes moisture enhanced subcritical crack growth (17,18). Direct crack growth measurements by Freiman et al (17) and Bruce et al (18) show that the rate of crack growth is dependent on the

partial pressure of water in the environment and the test temperature. The slopes of the crack velocity-K_I curves determined directly. as above, are in good agreement with those obtained through stressing rate procedures (19). Bruce et al (18) also showed that the slope and position of the crack growth curves for a PZT III ceramic were also a function of whether the material had been poled parallel or perpendicular to the crack plane. A more recent of analysis of the data of Bruce et al has suggested that the elastic anisotropy produced by the poling, rather than changes in the piezoelectric properties of the material, is the major determinant of their observed difference in crack growth (20). Finally. McHenry and Koepke (21) showed that the application of an electric field perpendicular to the crack plane in PZT strongly affected crack propagation behavior; V-K_I curves were shifted to lower K_I's with increasing applied voltage.

As an illustration that fracture of piezoelectric ceramics can occur, not only due to purely mechanical loads, but because of the electroelastic nature of the material, we refer to the work of Pohanka et al (22). These authors showed that driving PZT specimens at a resonant frequency could produce mechanical failure if the applied voltage was sufficiently high. The fracture stress produced by both single and multiple tone bursts was in excellent agreement with that predicted from flexural strength data. However, cw excitation produced failures at stresses lower than would have been predicted from the flaw sizes. Pohanka et al suggested that a fatigue mechanism of some type must be taking place to account for this behavior.

SUMMARY

Although we clearly do not have all of the answers to the problem of the mechanical failure of electronic ceramics, work produced over the past few years permits us to make some general statements regarding this phenomenon. One of the clearest results is that while the fracture toughness of these materials in the erroelectric state is larger than that in the paraelectric state, the strength follows an opposite trend. This difference in behavior is interpreted in terms of the size of the crack appropriate to strength or K_{IC} measurements. The experimental results obtained to date suggest that when the crack is small relative to the grain size in the material, i.e. $c \leq 3G$, local microstructural tensile stresses generated during the paraelectric to ferroelectric phase transformation at the Curie point act as an additional driving force for fracture, thereby reducing the measured strength. At larger crack sizes, these tensile stresses are by necessity balanced by compressive stresses formed at the same time, so that throughout the whole body, the net stress is zero. The magnitude of these stresses determined by strength measurements is in excellent agreement with that predicted from dielectric theory. Preliminary data suggest that correlations can be drawn between the effect of these internal stresses on strength and the dielectric aging rate of a capacitor material (22).

The crack growth resistance of ferroelectric materials is governed by many factors, including grain size, grain boundary chemistry, and the crystal phase distribution. Contributions to fracture toughness include crack-twin inter-actions, crack deflection, microcracking, and phase transformations at

crack tips. Quantitative models involving some of these processes have been developed, but much more work is needed.

At present, no clear picture exists of the effects of an electric field on fracture. Electric fields such as would be present during the operation of dielectric or ferroelectric devices could affect fracture in a number of ways, e.g., changing the domain orientation, producing additional stresses due to piezoelectric or electrostrictive behavior, or causing elastic anisotropy. Only a few experiments involving cyclically applied stresses have been performed (22,23). Results of these studies suggest that phenomena other than those occurring under static loads may be responsible for the failure of piezoelectric ceramics under more complex stressing conditions. Environmentally enhanced crack growth occurs in all piezoelectric ceramics due to the stress aided reaction of water with the atomic bonds at the crack tip. However, there are indications from some of the data on capacitor materials that a crack growth limit may exist, below which subcritical crack extension does not take place. The susceptibility of a particular material to environmentally enhanced crack growth seems to depend strongly on chemical composition, particularly that of the grain boundaries. Further knowledge of this phenomenon could help the component designer choose materials on the basis of mechanical reliability as well as electrical properties.

ACKNOWLEDGMENT

Much of the work performed by the author has been supported by the Office of Naval Research and by Sandia National Laboratories. The many helpful discussions with Bob Pohanka are gratefully acknowledged.

REFERENCES

1. Pohanka, R. C., C., R. W. Rice, and B. E. Walker, Jr., J. Am. Ceram. Soc. 59, 71-4 (1976)

2. Buessem, W. R., L. E. Cross, and A. K. Goswami, J. Am. Ceram. Soc. 49, 33-6 (1966)

3. Cook, R. F., S. W. Freiman, B. R. Lawn, and R. C. Pohanka, Ferroelectrics 50, 267-72 (1983)

4. Chantikul, P., G. R. Anstis, B. R. Lawn, and D. B. Marshall, J. Am. Ceram. Soc. 64 539-43 (1981)

5. Pohanka, R. C., S. W. Freiman, and B. A. Bender, J. Am. Ceram. Soc. 61, 72-5(1978)

6. de With, G., and J. E. D. Parren, Silicates Industriels 9 179-83 (1984)

7. Pohanka, R. C., S. W. Freiman, K. Okazaki, and S. Tashiro, Fracture Mechanics of Ceramics 5, 353-64, ed. by R. C. Bradt, A. G. Evans, D. P. H. Hasselman, and F. F. Lange, Plenum Press, New York (1983)

8. Rice, R. W. and S. W. Freiman, J. Am. Ceram. Soc. 64 350-4 (1981)

9. Baker, T. L. and S. W. Freiman, Electronic Packaging Materials Science 72 81-90, ed. by K. A. Jackson, R. C. Pohanka, D. R. Uhlmann, and D. R. Ulrich, Materials Research Soc., Pittsburgh (1986)

10. Jaffe, B., W. R. Cook, and H.Jaffe, "Piezoelectric Ceramics", p. 136 Academic Press, New York (1971)

11. Freiman, S. W., L. Chuck, J. J. Mechlsky, D. L. Shelleman, and L. J. Storz, Fracture Mechanics of Ceramics 8 175-85 ed. by R. C. Bradt, D. P. H. Hasselman. A. G. Evans and F. F. Lange, Plenum Press, New York (1986)

12. Tashiro, S., Igarashi, and K. Okazaki, Jpn. J. Appl. Phys. 20 197-203 (1981)

13. Fritz, I. J., and J. D. Keck, J. Phys. Chem. Solids. 39 1163-7 (1978)

14. Kuroda, K., and A. H. Heuer, Proc. of 41st Annual Meeting of Micros. Soc. of America. San Francisco Press, San Francisco (1983)

15. Spears, R. K., Ferroelectrics 37 653-6 (1981)

16. Dungan, R. H., and L. J. Storz, J. Am. Ceram. Soc. 68 530-3 (1985)

17. Freiman, S. W., K. R. McKinney and H. L. Smith, Fracture Mechanics of Ceramics 2 659 -76, ed. by R. C. Bradt. D. P. H. Hasselman and F. F. Lange, Plenum Press, New York (1974)

18. Bruce, J. G., W. W. Gerberich, and B. G. Koepke, Fracture Mechanics of Ceramics 4 687-709, ed. by R. C. Bradt, D. P. H. Hasselman, and F. F. Lange Plenum Press, New York (1978)

19. Caldwell, R. F., and R. C. Bradt, J. Am. Ceram. Soc. 60 168-70 (1977)

20. Pisarenko, G. G., V. M. Chushko, and S. Kovalev, J. Am. Ceram. Soc. 68 259-65 (1985)

21. McHenry, K. D., and B. G. Koepke, Fracture Mechanics of Ceramics 5, ed. by R. C.Bradt, A. G. Evans, D. P. H. Hasselman, and F. F. Lange, Plenum Press, New York (1983)

22. Pohanka, R. C., P. L. Smith, and J. Pasternak, Ferroelectrics 50 285-91 (1983)

23. Takahashi, S., E. Mori, Y. Tsuda. S. Kaneko, M. Ide and E. Ohiro, J. Acoustic Soc. Japan 28 241-51 (1972)

Figure Captions

Figure 1. Flexural strength of a laboratory prepared barium titanate as a function of grain size, G. Measurements were made in silicone oil at 25° C or above the Curie temperature at 150° C. The numbers of specimens per data point are shown in parentheses (after Pohanka et al (1).

Figure 2. Flexural strength of a commercial barium titanate tested above and below the Curie temperature as a function of the Curie temperature as a function of the indentation load used to introduce the flaw. All failures occurred from the indentation. The straight lines through the data at 25° C and 150° C represent the best fit line of slope, -1/3, following the indentation-fracture model (4). The deviation in the 25° C data from the model is ascribed to the contribution of internal stresses (after Cook et al (3)).

Figure 3. Critical fracture energy of barium titanate as a function of grain size at both 25° C and 150° C. Solid curve is the best fit to the 25° C data. The dashed line represents the model derived by Rice and Freiman (8). Note that the 150° C fracture energy of all the materials is independent of grain size (after Pohanka et al (7)).

Figure 4. Stressing rate dependence of the strength of a commercial barium titanate (same material as in Figure 2) tested in water at 25° C. The material was indented with a 30N load before testing. Crosshatched area is the strength under rapid loading in inert conditions. The slope of the curve is a measure of the materials susceptibility to moisture enhanced crack growth (after Cook et at (3)).

Figure 5. Critical fracture toughness, K_{IC}, of PZT as a function of the $PbTiO_3$ in the material. The vertical lines represent the positions of the phase boundaries (after Freiman et al (11)).

Figure 6. Indentation-fracture data for a 95/5 PZT ceramic $[Pb_yNb_{.02}(Zr_{.96}Ti_{.04})_{.98}O_3]$ in which y varied from 0.96 to 1.01. Positions of the curves of slope, -1/3, are indicative of the K_{IC} of each material. Strength plateaus are a measure of the effect of internal stresses (after Freiman et al (11)).

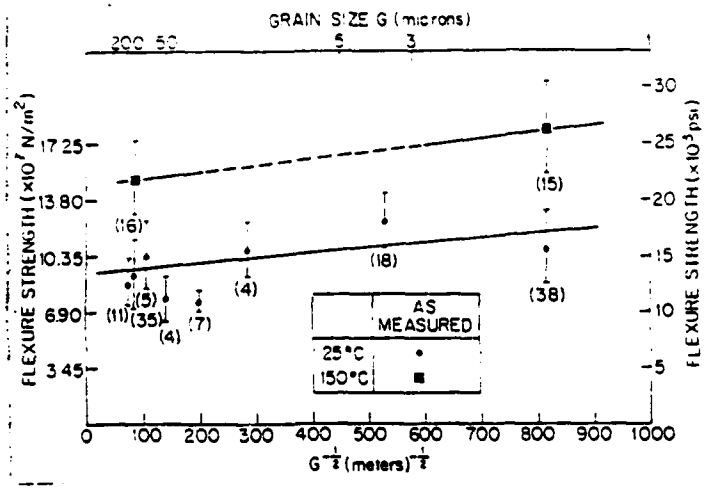

Figure 1

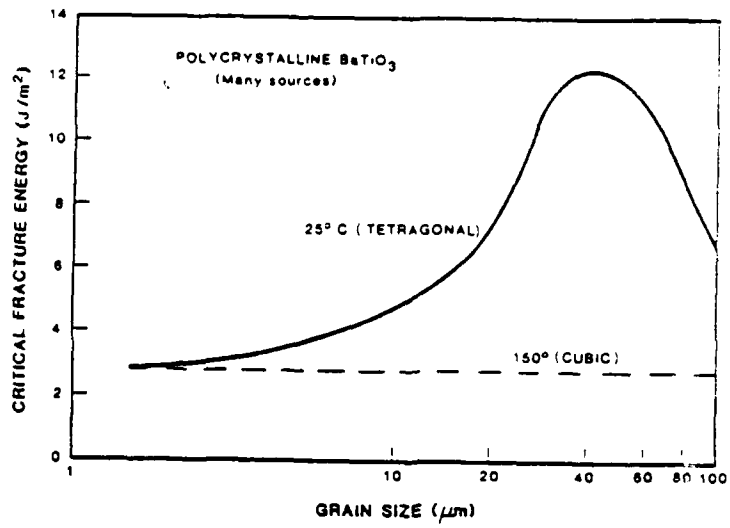

Figure 3

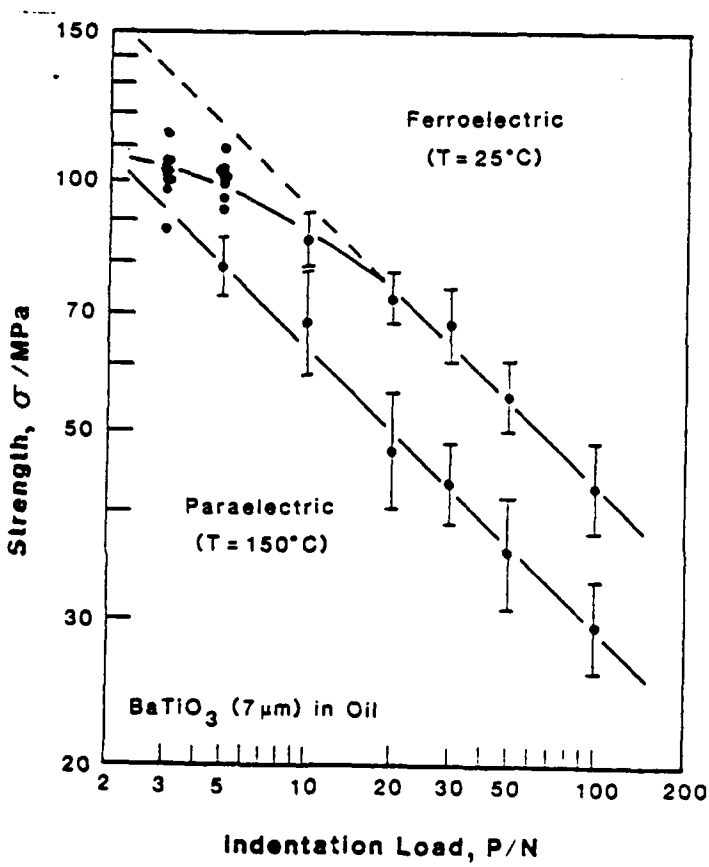

Figure 2

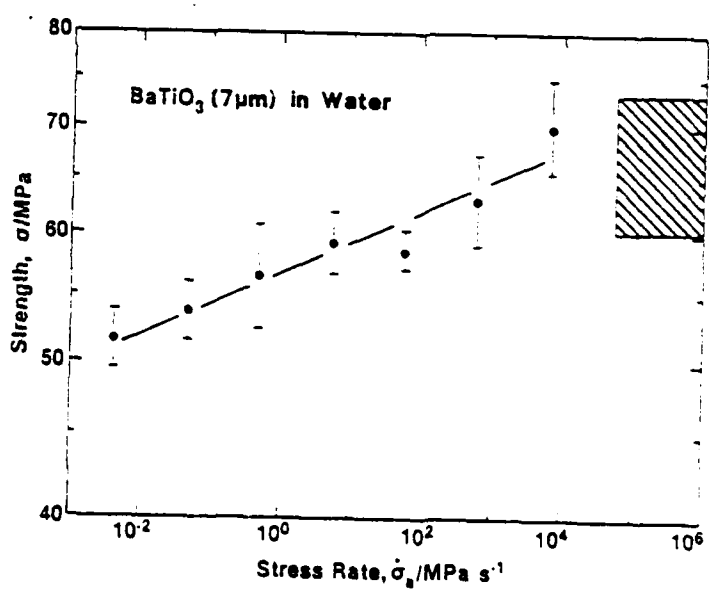

Figure 4

SECURITY CLASSIFICATION OF THIS PAGE (When Data Entered)

REPORT DOCUMENTATION PAGE

READ INSTRUCTIONS BEFORE COMPLETING FORM

1. REPORT NUMBER	2. GOVT ACCESSION NO. / 3. RECIPIENT'S CATALOG NUMBER
4. TITLE (and Subtitle): Stress Corrosion of Ceramic Materials	5. TYPE OF REPORT & PERIOD COVERED: Annual, 1 Oct 1986 - 31 Sept 1987
	6. PERFORMING ORG. REPORT NUMBER
7. AUTHOR(s): S. W. Freiman, G.S. White, T.R. Palamides, M. L. Balmer, A.M. Wilson, D.C. Cranmer, and C. Nguyen	8. CONTRACT OR GRANT NUMBER(s): N00014-87-F-0007
9. PERFORMING ORGANIZATION NAME AND ADDRESS: National Bureau of Standards, Ceramics Division, Rm A329, Bldg. 223, Gaithersburg, MD 20899	10. PROGRAM ELEMENT, PROJECT, TASK AREA & WORK UNIT NUMBERS
11. CONTROLLING OFFICE NAME AND ADDRESS	12. REPORT DATE: 10 January 1988
	13. NUMBER OF PAGES
14. MONITORING AGENCY NAME & ADDRESS (if different from Controlling Office)	15. SECURITY CLASS. (of this report)
	15a. DECLASSIFICATION/DOWNGRADING SCHEDULE

16. DISTRIBUTION STATEMENT (of this Report)

17. DISTRIBUTION STATEMENT (of the abstract entered in Block 20, if different from Report)

18. SUPPLEMENTARY NOTES

19. KEY WORDS (Continue on reverse side if necessary and identify by block number)

crack growth; fracture; stress corrosion; ceramics, silicon, gallium arsenide; capacitors; dielectric aging

20. ABSTRACT (Continue on reverse side if necessary and identify by block number)

Environmentally enhanced crack growth data was obtained for GaAs in a number of chemical environments. The effectiveness of particular environments was predicted on the basis of existing crack growth models. No environment was found to produce crack growth in silicon. Dielectric aging studies were conducted on capacitor ceramics. A correlation was shown between decreases in dielectric constant and reductions in identation strength at small indentation loads.

DD FORM 1 JAN 73 1473 EDITION OF 1 NOV 65 IS OBSOLETE
S/N 0102-LF-014-6601

SECURITY CLASSIFICATION OF THIS PAGE (When Data Entered)

END

DATE

FILMED

5-88

DTIC